Model-Based Motion Control for Multi-Axis Servohydraulic Shaking Tables

A.R.Plummer
Centre for Power Transmission and Motion Control
Department of Mechanical Engineering
University of Bath
Bath BA2 7AY, UK
A.R.Plummer@bath.ac.uk

ABSTRACT

The shaking table is an essential testing tool in the development of earthquake resistant buildings and infrastructure, so improving its performance is an important contribution to saving lives. Currently the bandwidth and accuracy of shaking tables is such that earthquake motion often cannot be replicated with the desired fidelity. A new model-based motion control method is presented for multi-axis shaking tables. The ability of this method to decouple the control axes is demonstrated. A linear parameter varying modal control approach is used – i.e. the modes of vibration of the system are controlled individually, with the modal decomposition repeated at each time step to account for parameter variations. For each mode, a partial non-linear dynamic inversion is performed in the control loop. Feedback is based on a combination of position and acceleration measurements. A command feedforward method is proposed to increase the tracking bandwidth, thus the controller has a two degree-of-freedom structure. Experimental and simulation results are presented for a large (43 tonne total) six degree-of-freedom shaking table. The simulation results are based on a detailed, validated model of the table. Experimental results show that the controller gives exceptional performance compared a conventional proportional controller: for example the horizontal acceleration bandwidth is six-times higher at over 100Hz, which is also many times higher than the hydraulic resonant frequency. These results will allow a step change in earthquake simulation accuracy.

KEYWORDS: shaking table, electrohydraulic servosystem, earthquake simulation, multi-axis control, parallel kinematic mechanism, modal control.

NOMENCLATURE

${}^{c}\boldsymbol{a}_t$	Table acceleration vector in Cartesian space
A	Piston area
$A(s)$	Actuator second order characteristic polynomial
$A_1(s)$	Product of $A(s)$ and h
$\mathbf{B}$	Diagonal damping matrix
c	Actuator damping
${}^{w}c_{ox}$	x coordinate of origin of frame {C} defined in frame {W}
${}^{w}c_{oy}$	y coordinate of origin of frame {C} defined in frame {W}
${}^{w}c_{oz}$	z coordinate of origin of frame {C} defined in frame {W}
d_i	Disturbance for axis i
$\mathbf{D}$	Actuator to internal (or deformation) force transformation
${}^{c}\boldsymbol{f}_t$	Table force vector in Cartesian space
f_h	Actuator force (product of pressure different and piston area)
F_{stall}	Actuator stall force
g	Estimate of ratio H_0/h used to scale control signal in final controller
$G(s)$	Low pass motion estimation filter
h	Valve/actuator velocity gain
h_c	Centre of gravity height
H_0	Maximum value of h.
I_x, I_y, I_z	Moments of inertia about axes x, y, z
$\mathbf{I}$	Identity matrix
$\mathbf{I_t}$	3x3 moment of inertia matrix
$\mathbf{J_i}$	Jacobian relating actuator body to table velocity vectors
k	Actuator stiffness
k_p	Proportional gain
k_{pi}	Proportional gain, position axis i
k_{pf}	Proportional gain, force axis
K_m	Actuator mounting stiffness
K_c	Actuator pushrod stiffness
$\mathbf{K}$	Stiffness matrix
L_h	Horizontal (x) actuator offset from table centre line

L_v	Vertical (z) actuator offset from table centre line
m	Mass moved by actuator
m_t	Mass of table and payload
$\mathbf{M}$	Total mass matrix in frame {C}
$\mathbf{M_{ai}}$	Mass matrix of actuator body, actuator i
$\mathbf{M_c}$	Mass matrix of table in frame {C}
$\mathbf{M_{cg}}$	Mass matrix of table about centre of gravity
N	Number of actuators
p_1, p_2	Cylinder chamber pressures
p_{acc},	Accumulator hydraulic pressure
P_r,	Return hydraulic pressure
$\mathbf{P}$	Modal to Cartesian space transformation
q_1, q_2	Cylinder flowrates
$\mathbf{Q}$	Cartesian to actuator space transformation
r_i	Position command, axis i
r_s	Accumulator pressure, as a proportion of its maximum
$\mathbf{R}$	Modal to actuator space transformation
s	Differential operator
$\mathbf{u}$	Control signal
u_i	Control signal for actuator i
u_i'	Control signal for augmented plant, actuator i
u_i''	u_i' filtered by $A_1(s)$
v_i	Valve spool displacement for actuator i
$\mathbf{v}$	Vector of spool displacements
V_1, V_2	Cylinder chamber volumes
$V(s)$	Valve dynamics model
$W(s)$	Factor of augmented plant (without integrator)
x_i	'No-load' actuator displacement
$\mathbf{x}$	Vector of non-load actuator displacements
$\mathbf{y}$	Vector of actuator displacements
y_i	Effective displacement of actuator i
z_i	Displacement of piston i

Greek letters

δ	Valve dead time
ϕ	Roll (rotation about *x* axis)
θ	Pitch (rotation about *y* axis)
$\mathbf{\Omega}$	Diagonalised frequency matrix
τ_c	Characteristic time (delay)
ω_i	Natural frequency of modal axis *i*
ω_{nv}	Valve natural frequency
ψ	Yaw (rotation about *z* axis)
ζ	Valve damping ratio

Subscripts

c	Cartesian coordinates
m	Modal coordinates
i	For axis or actuator *i*

Diacritical mark

^	Estimate of

1. INTRODUCTION

Servohydraulic shaking tables are used to simulate earthquake-induced ground motion for the seismic testing of large structures. Such testing is a vital part of the development of earthquake resilient buildings and infrastructure (e.g. bridges and dams), and thus plays a part in safeguarding many thousands of lives. However the control of shaking tables to accurately replicate the desired motion is a very significant challenge. This is due to both the high bandwidth requirements, and the desire for simultaneous multi-axis control with minimal cross-coupling. This paper presents, for the first time, a linear-parameter-varying modal controller which is shown in practice to achieve high bandwidth multi-axis control for a large six degree-of-freedom over-constrained shaking table.

Fig. 1 shows a typical arrangement for a 6 degree-of-freedom (DOF) multi-axis shaking table with a payload capacity of a few hundred kilograms. Such tables are used for a range of multi-axis vibration testing tasks, not only for earthquake simulation. Servohydraulic actuators provide high force and acceleration with relatively low mass and size. A parallel kinematic arrangement of servohydraulic actuators provides greater stiffness than a serial connection of actuators, and hence the potential for multi-axis motion with the highest achievable dynamic response. Larger tables are often preferred for earthquake testing of model buildings so that the scale factors are not so extreme; these can typically accommodate payloads of at least several tonnes. Fig. 2 shows an example at the IWHR research institute in Beijing, for which results are presented in this paper. The Japanese E-defense facility commissioned in 2006 is the world's largest shaking table can handle payloads up to 1200 tonnes – large enough for the testing of four-storey buildings at full scale [1]. In a very large table such as this high mass is moved by long-stroke actuators, giving low hydraulic resonant frequencies; the E-defense table with a 1200 tonne payload has resonant frequencies in the range 3Hz to 8Hz, yet the aspiration for earthquake simulation is for accurate control up to 15Hz, presenting a significant controller design challenge [1]. Alternatively, if a scale model of the test structure is used with a smaller table, this necessitates compressing the timescale of the earthquake signal and hence demands a higher bandwidth for the closed-loop system. The need to operate at frequencies beyond the hydraulic resonance is an unusual and difficult problem for hydraulic servo engineers, and compensation for this characteristic is essential [2]. The servo-valve response, particularly its phase lag, will also have a significant impact, and a high performance controller cannot be designed without accounting for it. Further, a high centre of gravity and large horizontal accelerations may be encountered, generating a large overturning moment which tends to cause the table to pitch. In many structural testing applications iterative control enables the best drive signals to learnt, but destructive seismic testing does not permit repeated trials, so the real-time control accuracy must be relied upon.

In this paper, a practical motion control method is presented for shaker tables. Modal control is used – i.e. the modes of vibration of the table are controlled individually, and this requires a parameter varying controller with on-line modal decomposition to account for the variation of actuator stiffness with operating point. Many shaker tables are over-constrained, i.e. have more actuators than degrees-of-freedom in order to spread the actuation loads, and thus internal force control is used to prevent actuators 'fighting' one another; in this work the measured forces are transformed to force control axes which formally complement the modal motion coordinates. A model-based feedforward scheme is also developed. The performance of the approach is demonstrated for the 6 DOF shaking table shown in Fig. 2, both in simulation and experimentally.

A modal decoupling approach for shaking tables was first described in [3]. Simulation results were presented using a very simple (proportional plus lag) closed-loop compensator. A model-based controller was demonstrated for a 3-axis shaking table in simulation in [4]. Experimental research into multi-axis control of vibration tables is fairly sparse, although a number of uni-axial studies have been performed (e.g. [5,6]). An overview of shaking table control schemes is presented in [7].

The published works on motion control of large multi-degree of freedom seismic testing tables which do exist have been mostly undertaken in Japan. This has been motivated by the Japanese government's investment in large-scale testing facilities following the Hanshin-Awaji earthquake at Kobe in 1995 [1].

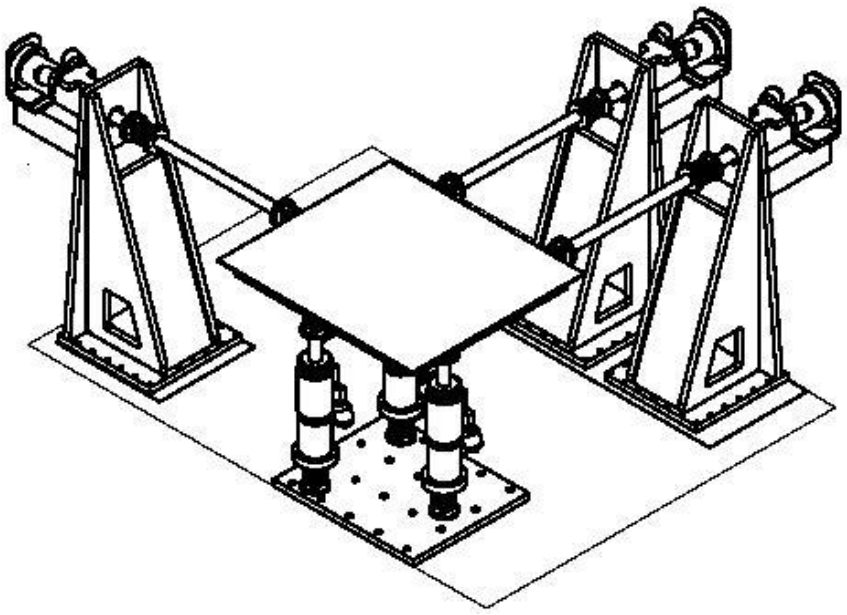

Fig. 1 A 6 DOF multi-axis shaking table with 1.5m square table, 6 actuators, 0.5 tonne capacity.

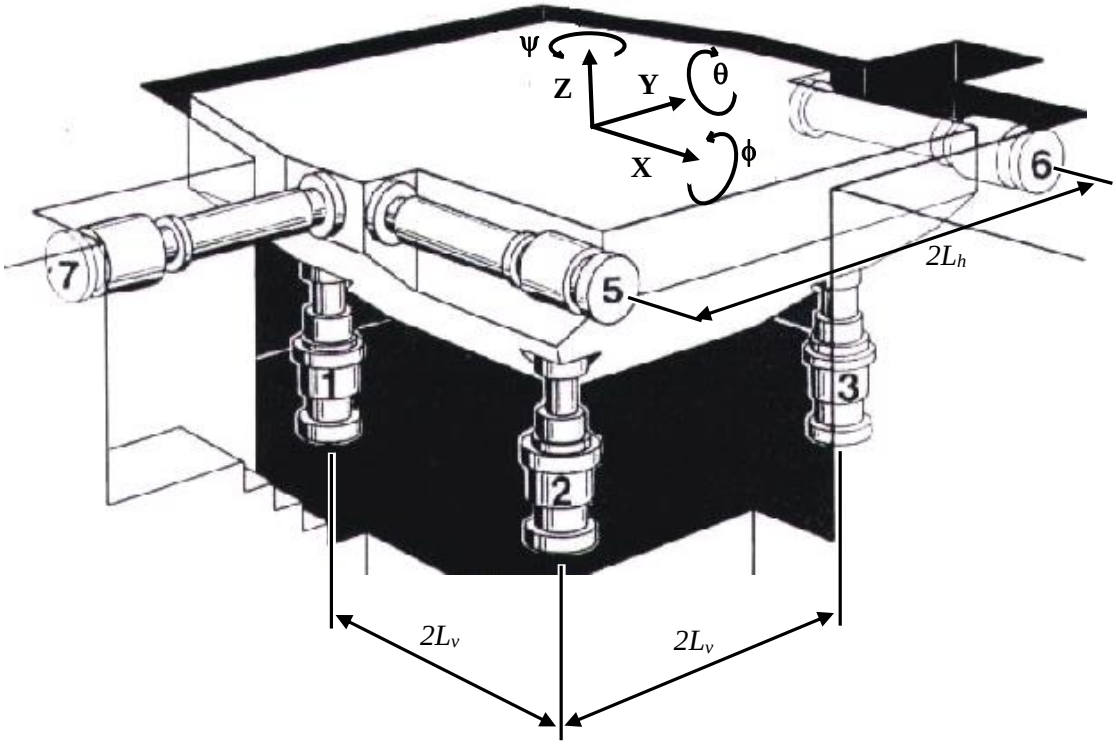

(a) The arrangement of actuators.

(b) The shaking table laboratory, with mast test specimen on the table.

Fig. 2 A 5m x 5m 6 DOF shaking table with 7 actuators and 20 tonne capacity.

Although iterative control is often used to obtain the required base accelerations, many tests involve the failure or partial failure of the specimen, and thus iteration cannot be used in these cases [2]. Hence improvements in closed-loop control have been sought.

Proportional-integral (PI) positional control, sometimes with acceleration or differential pressure feedback, has often been used for this application in the past. However, Three-Variable Control is now becoming common, increasing flexibility and providing command feedforward to improve the bandwidth [2,8]. In current practice, tuning the controller depends on the expertise of the operator; however a model-based pole-placement tuning method is proposed in [9], and an approach using an inverse-model is described in [10].

Recently, attention has been given to model-based design of the command feedforward term. Philips *et al* [11] use acceleration feedforward to improve the tracking response of a Linear Quadratic Gaussian feedback controller. Nakata [12] has also proposed and experimentally verified the use of a model-based acceleration feedforward term, and similarly to the present paper delays the command to the feedback loop to improve synchronization of feedforward and feedback control action.

Adaptive control has been studied for shaking tables, which has the attractive potential of adapting to new specimens or changes within an existing specimen during testing. Trials with first order MCS (Minimal Control Synthesis) are described by Stoten and Gomez [13] for two shaking tables. First order MCS provides adaptive tuning of gains in a proportional or PI controller, and can be used alone, or (as for the results shown) in conjunction with an existing fixed gain controller. Tests include 1Hz or 2Hz sinusoidal commands, and earthquake signals with frequency content up to around 6Hz. Similarly, some improvement in tracking response is demonstrated using MCS compared to a detuned fixed controller in [14], where both one and two-axis control of a 40 tonne table with a 41 tonne flexible specimen are described. The same MCS algorithm has also been used to adaptively tune a command signal filter to improve tracking response [15]. Another study by Shen *et al* [16] has used a combination of off-line and adaptive inverse modelling to control one axis of a shaking table. An adaptive command filter is shown to work well experimentally for a 2 DOF table in [17]; this table has four actuators and so is overconstrained, and the benefit of using internal force control is demonstrated.

A novel approach to reducing the influence of the specimen on the table response is introduced in [18]. Specimen force is measured and fed forward to cancel force disturbance on a position loop. The full derivation is contained in [19], where a third-order lead term is used in the force feedforward signal as an

approximate inverse of the transfer function from valve drive to specimen force. Results are shown for a flexible 600kg specimen mounted on a small uni-axial shaking table, and the disturbance due to specimen resonance at either 3.8 Hz or 6.8Hz (depending on specimen configuration) is much reduced. A similar approach was patented in 1985 [20], but there is no evidence that it was used successfully at this time.

Four European shaking tables are reviewed in [21], with sizes between 3m and 5.6m square; the hydraulic resonances are mostly in the range 10 to 50Hz depending on axis and specimen. Real earthquake signals do not have significant frequency content above 8Hz [22], but the frequency must be scaled up when reduced-scale model buildings are tested, and many such shaking tables are required to test up to 100Hz. Thus the desire is to achieve acceptable motion tracking in a frequency range extending well beyond the hydraulic resonances.

This paper describes the derivation of a motion controller based on a physical model. Specifically, the final controller has the following key features which are found to be necessary to achieve excellent performance:

1. decomposition of multi-axis dynamic behavior into separate modes in real-time, based on mass matrix (fixed) and stiffness matrix (variable with piston position), and controlling modes explicitly,
2. a time-varying inverse second-order actuator model in the forward path (in modal co-ordinates), forming an 'augmented plant' in which the actuator dynamics are cancelled,
3. command velocity feedforward, and proportional feedback of a disturbance estimate (the difference between expected and actual motion), and the use of optimal motion estimation based on position and acceleration measurements,
4. force control for redundant actuators to keep internal loads small.

The time-varying multi-axis modal control and dynamic compensation described in points 1. and 2. are new methods, and the control structure of point 3. has not been applied to a multi-axis system before. The experimental demonstration of the combined approach applied to a substantial, commercial shaking table is a major original contribution.

Section 2 covers modeling and controller design for a single servohydraulic axis, including a preliminary robustness investigation. Motion measurement issues are also discussed. Section 3 extends the controller to the multi-axis case, where a modal control approach is used. Compensation for non-linearities, and the case where the number of actuators exceeds the number of degrees-of-freedom, are both considered. Section 4 describes the example shaking table, including simulation and experimental results.

2 SINGLE AXIS MODELLING AND CONTROL

2.1 Modelling

Firstly, the model of a single servovalve-controlled actuator driving an inertial load will be considered (Fig. 3). As shown in the Appendix, a linear model of the position response of the actuator is given by

$$y_i = \frac{1}{sA(s)} v_i \,, \tag{1}$$

where

$$A(s) = \frac{1}{h}\left(\frac{m}{k}s^2 + \frac{c}{k}s + 1\right), \tag{2}$$

and where y_i is the piston position, v_i is the valve spool position, m is the mass driven by the actuator, c is the effective damping, k is the hydraulic and mechanical stiffness and h is the steady state gain of actuator velocity over spool position. Also shown in the Appendix is that this can be considered a linearisation of a non-linear differential equation in which gain h is a function of load force and accumulator pressure (equation A24), and the stiffness k is a function of piston displacement (equation A28). It is assumed that the hydraulic resonant frequency given by equation (2) is the same order of magnitude as the valve bandwidth, so the valve dynamics cannot be ignored. The response of the valve spool position to control signal u_i can be approximated by this second order transfer function plus delay [22]:

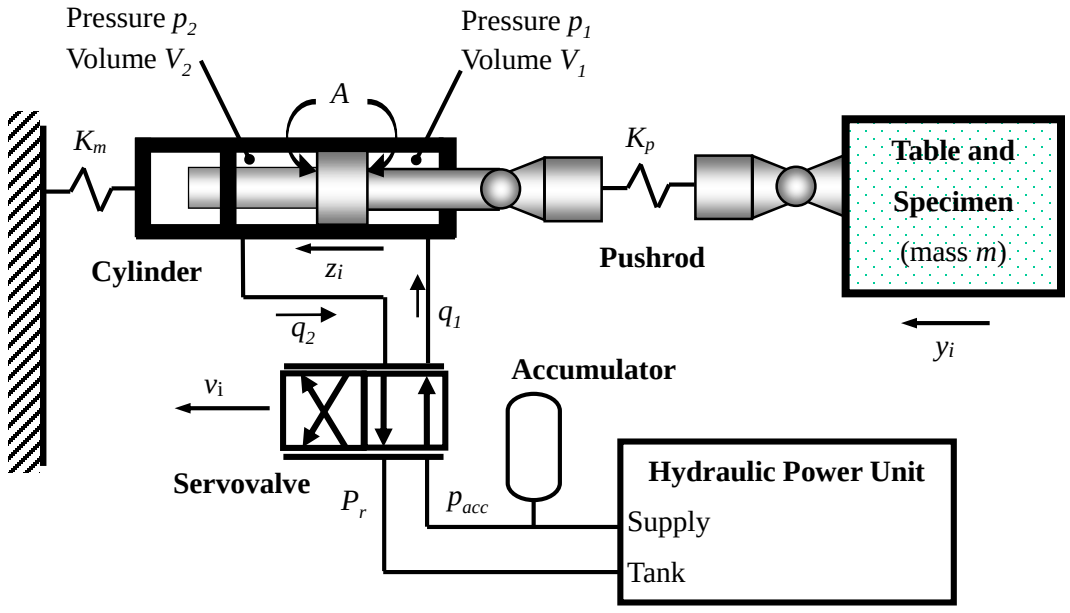

Fig. 3 An actuator showing the hydraulic parameters.

$$v_i = V(s)u_i\,, \tag{3}$$

where

$$V(s) = \frac{{\omega_{nv}}^2 e^{-s\delta}}{s^2 + 2\zeta\omega_{nv}s + {\omega_{nv}}^2}\,. \tag{4}$$

For example, Fig 4 shows a plant frequency response; this is the experimental Y-direction position response of the shaking table shown in Fig 2 and analyzed in Section 4. A best-fit model is shown for comparison. In this case the best-fit model parameters are: h = 53/s, m = 23 000kg, c = 1.20x10^6 Ns/m, k = 484x10^6 N/m, δ = 0.002s, ω_{nv} =754 rad/s, ζ = 0.70.

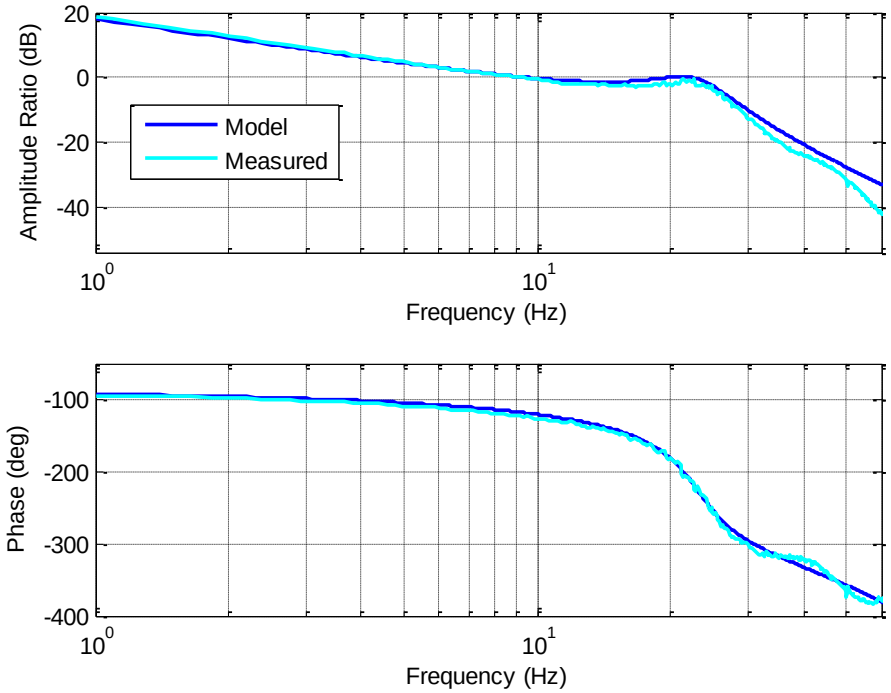

Fig 4. An example plant frequency response (input u_i, output y_i).

2.2 Controller design for augmented plant

A variety of methods can be used to design a controller for this type of system [2,23]. In this work, the model-based controller shown in Fig. 5 is proposed. It can be considered as having a command velocity feedforward path, and proportional feedback of a disturbance estimate. The filter $\hat{W}(s)$ is an estimate of the *W(s)* component of the augmented plant. The closed loop response is given by

$$y_i = \frac{s + k_p\hat{W}(s)}{s + k_p W(s)}W(s)r_i + \frac{s}{s + k_p W(s)}d_i\,. \tag{5}$$

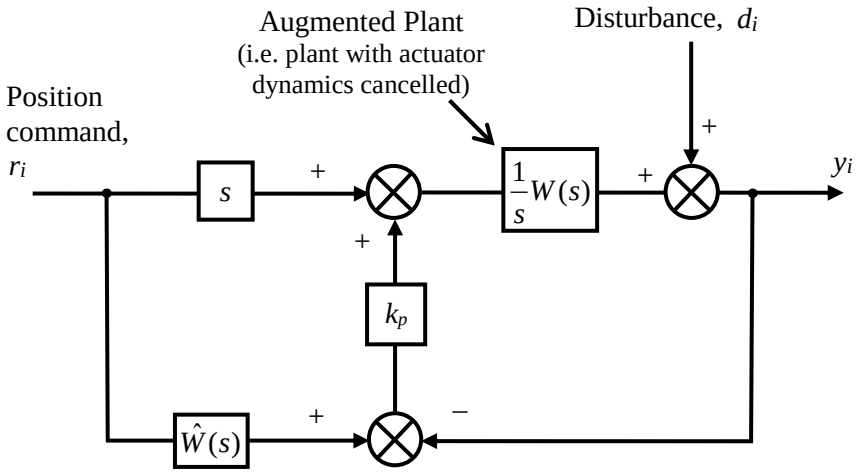

Fig. 5. The servohydraulic position control system for a single axis.

The augmented plant is the plant with the actuator dynamics cancelled out, and so its dynamic characteristics are those of the valve. The motivation for this is that, unlike the actuator dynamics, the valve dynamics should be well damped and so the augmented plant is amenable to a simply-tuned proportional controller. This is demonstrated in this Section, along with the method used for calculation the proportional gain. The detailed derivation of the augmented plant from the model of Section 2.1 is described in Section 2.3.

The augmented plant factor *W(s)* will be the second order lag plus delay of the valve. So from equation (4),

$$W(s) = \frac{{\omega_{nv}}^2 e^{-s\delta}}{s^2 + 2\zeta\omega_{nv}s + {\omega_{nv}}^2}\,. \tag{6}$$

The following heuristic rule will be adopted to calculate the proportional gain:

$$k_p = \frac{1}{2\hat{\tau}_c}\,, \tag{7}$$

where $\hat{\tau}_c$ is the estimate of a characteristic time τ_c given by

$$\tau_c = \frac{2\zeta}{\omega_{nv}} + \delta\,. \tag{8}$$

This rule stems from the fact that *W(s)* can be approximated by a deadtime of τ_c at frequencies well below ω_{nv}; controller design rules based on this type of model reduction are described in [20]. Each servovalve has its own closed loop controller, often with mechanical feedback, set up to achieve a desired spool dynamic response characteristic *V(s)*. Typically damping ζ will be in the range 0.7 to 1.0. Fig. 6 shows

disturbance step responses for some different combinations of delay and natural frequency with ζ = 0.7, using propotional gain given by equation (7), and assuming accurate knowledge of the plant ($\hat{\tau}_c = \tau_c$). Overshoot is in the range 4% to 8%.

Fig. 7 is an example of the variation in response with modelling error. In this example, there are errors in the estimate of delay and natural frequency amounting to a 20% error in the characteristic time estimate $\hat{\tau}_c$; this effects both $\hat{W}(s)$ and k_p.

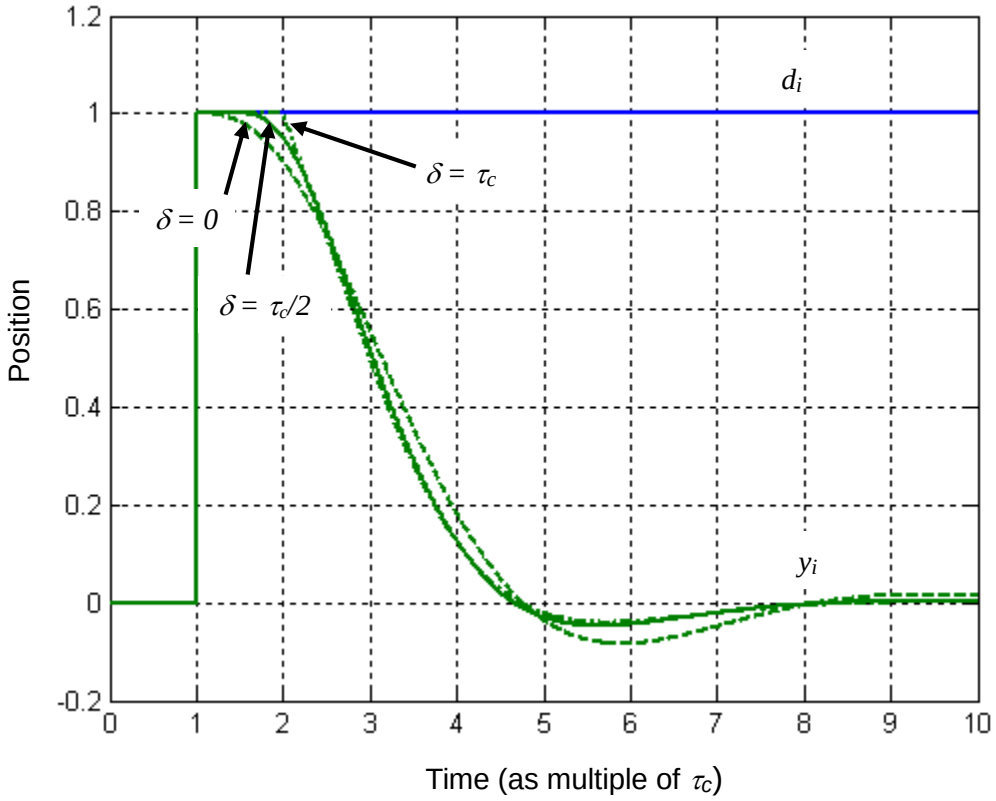

Fig. 6. Disturbance response examples.

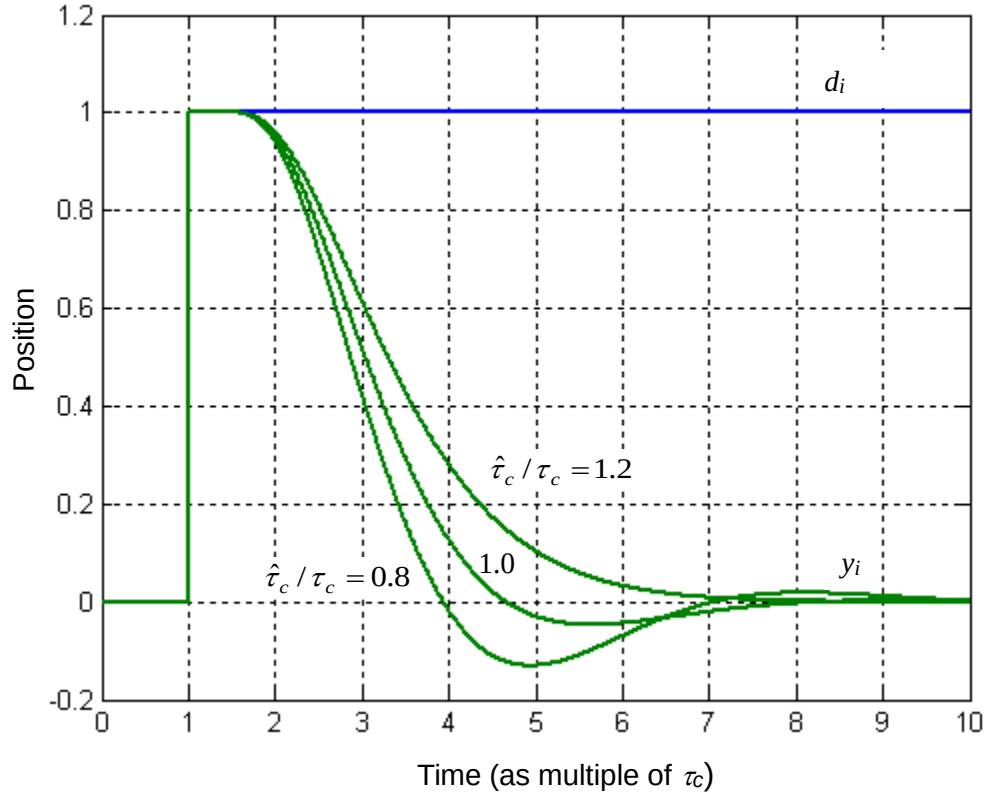

Fig. 7 The robustness of the disturbance response ($\delta = \tau_c/2$, ζ=0.7).

From equation (5) it is clear that the closed loop tracking response is identical to the augmented plant factor *W(s)* when $\hat{W}(s) = W(s)$. The effect of errors in the augmented plant model is shown in the tracking response to a step input in Fig. 8.

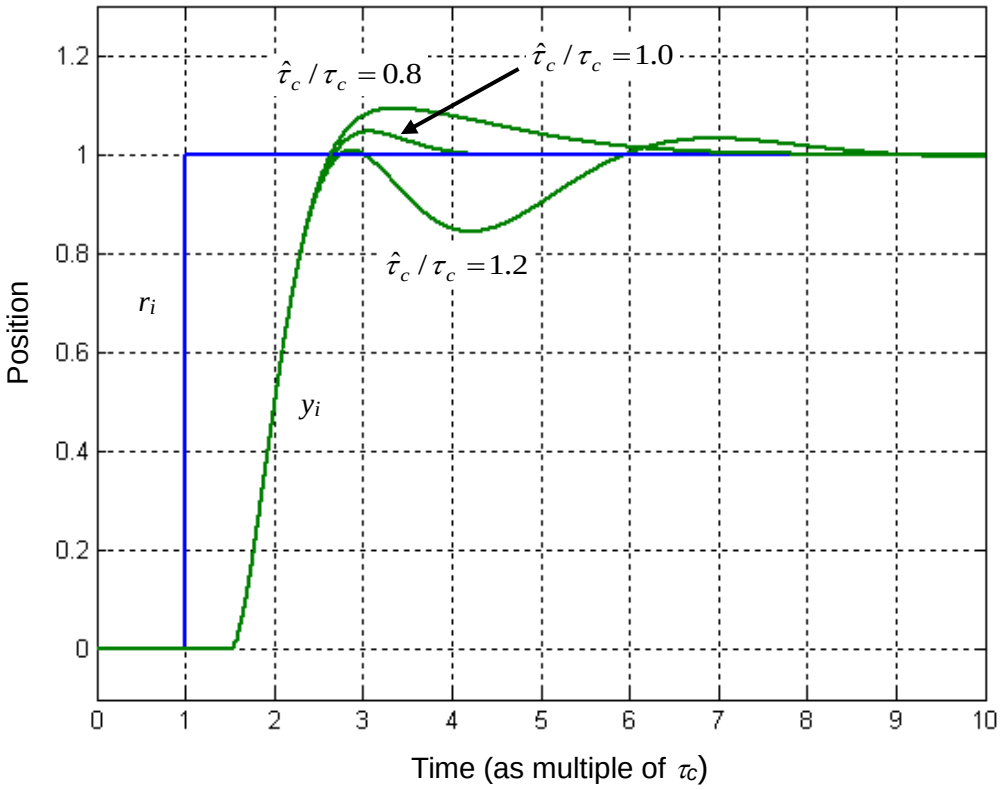

Fig. 8 The robustness of the tracking response ($\delta = \tau_c/2$, ζ=0.7).

2.3 Augmented plant

The augmented plant includes a compensator to cancel the second order lag in the actuator dynamics given in equation (1). The plant is

$$y_i = \frac{1}{sA(s)} V(s) u_i + d_i \tag{9}$$

and so including the inverse actuator model

$$u_i = \hat{A}(s) u_i' \tag{10}$$

gives the augmented plant $$y_i = \frac{1}{s} W'(s) u_i' + d_i, \tag{11}$$

where $$W'(s) = \frac{\hat{A}(s)}{A(s)} V(s), \tag{12}$$

and $\hat{A}(s)$ is an estimate of the actuator dynamics $A(s)$. Note that *W'(s)* would be the same as *W(s)* if there were no error in the actuator dynamics modelling.

Fig. 9 shows the controller including the inverse actuator model. The inverse actuator model can be split into

$$\hat{A}(s) = \frac{1}{\hat{h}(p_{acc}, \ddot{r}_i, u_i'')} \hat{A}_1(s), \tag{13}$$

where $$\hat{A}_1(s) = \frac{\hat{m}}{\hat{k}(z_i)} s^2 + \frac{\hat{c}}{\hat{k}(z_i)} s + 1 \tag{14}$$

and $$u_i'' = \hat{A}_1(s) u_i'. \tag{15}$$

As indicated in equation (14), a variable stiffness is used in the inverse actuator model, the value being dependent on the piston position according to equation (A28). In addition, a variable gain value is used in equation (13), estimated in line with equation (A24). However in the latter equation, the current actuator force f_h is required, along with the current spool position v_i. As there is a lag in applying the gain correction to the actuator due to the valve response characteristic, a prediction of future values of these variables is appropriate. The actuator force will be predicted using the product of command acceleration and mass, and u_i'' will be used as a prediction of v_i. The accumulator pressure p_{acc} is also required (expressed as a ratio r_s, equation (A22)), and it is assumed that this is measured. Hence,

$$\hat{h}(p_{acc}, \ddot{r}_i, u_i'') = \hat{H}_0 \sqrt{\hat{r}_s \left(1 - \frac{\hat{m} \ddot{r}_i}{\hat{r}_s \hat{F}_{stall}} \operatorname{sgn}(u_i'') \right)}. \tag{16}$$

To illustrate the robustness of the controller in relation to errors in the inverse actuator model, consider the case where there are only modelling errors in $\hat{A}_1(s)$. Figures 11 and 12 illustrate the effect on the closed loop step response of errors in the first and second coefficients in equation (14). A larger (50%) error in damping coefficient estimate $\hat{c}$ is shown as this is likely to be harder to estimate, and in reality will vary. These results are for a valve *V(s)* which has $\delta = \tau_c/2$ and ζ=0.7, and an actuator *A(s)* with a damping ratio of 0.2 and a natural frequency 10% of the valve natural frequency ω_{nv}. These actuator parameters are similar to those for the experimental system described later in the paper.

2.4 Position measurement

The objective is to control the motion of the table; in fact, although position y_i is shown as the controlled variable, it is the acceleration $\ddot{y}_i$ which is of most concern for this type of vibration test equipment. Typically, the only position measurement available is from a sensor attached to the hydraulic cylinder, providing a measurement of relative piston-to-cylinder position (z_i in Fig. 3).

As implied by equation (10), there is a requirement for generating first and second derivatives from the position signal, and thus the measurement noise must reduce with increasing frequency. It is assumed that there is no direct measurement of table position (only relative piston-to-cylinder position z_i), however it is straightforward to measure acceleration $\ddot{y}_i$ using a table-mounted accelerometer. Position z_i is a reasonable estimate of table position at low frequency when the inertial forces are small, but not so at higher frequencies due to compliance in the cylinder mounting and the pushrod and joints forming the table connection. Acceleration and position measurements are combined to estimate table position thus:

$$\hat{y}_i = G(s)z_m + \frac{1-G(s)}{s^2}\ddot{y}_m \,. \tag{17}$$

where $\ddot{y}_m$ and z_m are measurements of table acceleration and relative piston-to-cylinder displacement. The form of the low pass filter *G(s)* is important to ensure the accuracy of the resulting estimate, and it is designed according to[25].

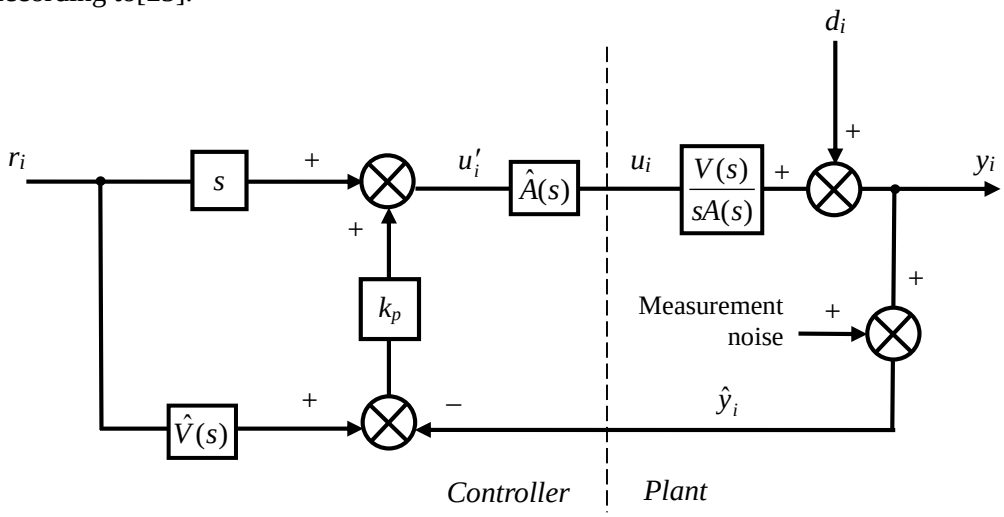

Fig. 9. The single axis position control system, including plant augmentation using the inverse actuator model.

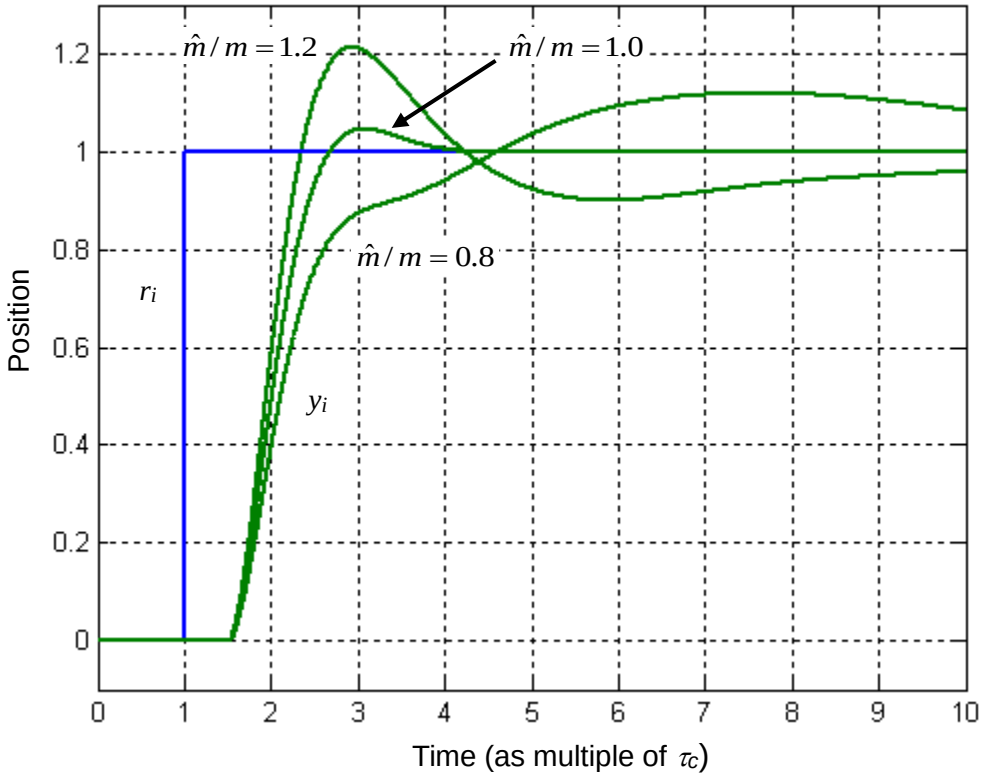

Fig. 10. The robustness of the tracking response to error in inverse actuator model parameter $\hat{m}$.

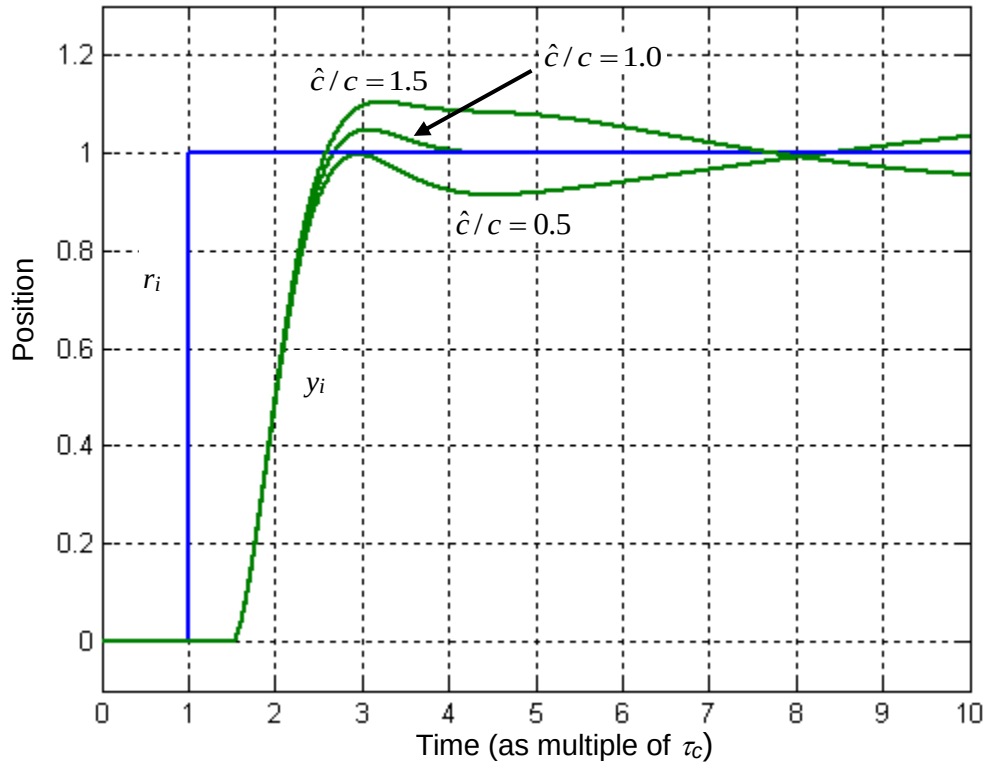

Fig. 11. The robustness of the tracking response to error in inverse actuator model parameter $\hat{c}$.

3 MULTI-AXIS MODAL CONTROL

3.1 Linear model and decoupling control

A linear multi-axis model can be derived as an extension of the single axis model. The derivation is shown for a six degree-of-freedom (DOF) motion system, although the approach is not limited to such a system. Shaker tables have a fairly small range of motion, so that the geometry-related non-linearities do not have a significant influence on the dynamic properties, and will be neglected. For an N actuator table ($N \geq 6$), column vectors **y, v** and **u** will be used to represent all actuator displacements, valve spool displacements, and control signals respectively, with sequential elements y_i, v_i and u_i respectively for individual actuators, where $i = 1$ to N. Six element column vector $\mathbf{y_c}$ will be used to indicate table position defined in Cartesian co-ordinates, and a matrix **Q** introduced as the linear algebraic transformation from Cartesian to actuator space (i.e. $\mathbf{y_c}$ to **y**). The same transformation defines the the relationship between other quantities expressed in Cartesian space, denoted with subscript **c**, and actuator space, e.g. between $\mathbf{u_c}$ and **u**. A modal decomposition will also be introduced, and subscript **m** will be used to indicate vectors defined in modal space, thus $\mathbf{y_m}$ is the six element column vector of modal displacements, and $\mathbf{u_m}$ is the modal control signal vector of the same dimensions. A matrix **P** will be introduced giving the linear transformation from modal to cartesian space, and matrix **R** transforms from modal to actuator space.

First, reconsider equations (1) and (2). Defining x_i to be the 'no load' actuator position,

$$x_i = \frac{h}{s} v_i \,. \tag{18}$$

The damping term, which originates from hydraulic leakage (see Appendix) is expected to be small [2]. So neglecting this term,

$$y_i = \frac{k}{ms^2 + k} x_i \,, \tag{19}$$

or

$$ms^2 y_i + k(y_i - x_i) = 0 \,. \tag{20}$$

For a 6 DOF table, a *6*x*6* mass matrix **M** can be derived relating small perturbations in table acceleration to total table force, and a 6x6 stiffness matrix **K** can be derived relating small perturbations in table postion to external table force. Table motion and forces are defined in terms of three orthogonal linear axes (*X,Y,Z*) and three orthogonal rotary axes (roll ϕ, pitch θ and yaw ψ Euler angles) of a table-fixed frame {C} relative to a world frame (see Fig. 12). The calculation of **M** and **K** are described in section 3.2. If these are found for the mid-position of the table, then the multi-axis model linearized about this mid-position is

$$\mathbf{M}s^2\mathbf{y_c} + \mathbf{K}(\mathbf{y_c} - \mathbf{x_c}) = 0, \tag{21}$$

or

$$s^2\mathbf{y_c} + \mathbf{M}^{-1}\mathbf{K}(\mathbf{y_c} - \mathbf{x_c}) = 0, \tag{22}$$

where $\mathbf{y_c}$ is the vector of 6 table Cartesian displacements (linear and angular) of frame {C}, i.e.

$$\mathbf{y_c} = \begin{bmatrix} {}^W c_{ox} & {}^W c_{oy} & {}^W c_{oz} & \phi & \theta & \psi \end{bmatrix}^T, \tag{23}$$

and $\mathbf{x_c}$ is the equivalent vector of 6 no load displacements, defined as the table displacement $\mathbf{y_c}$ which would occur if the actuators were insensitive to force and thus dictated only be the valve spool positions.

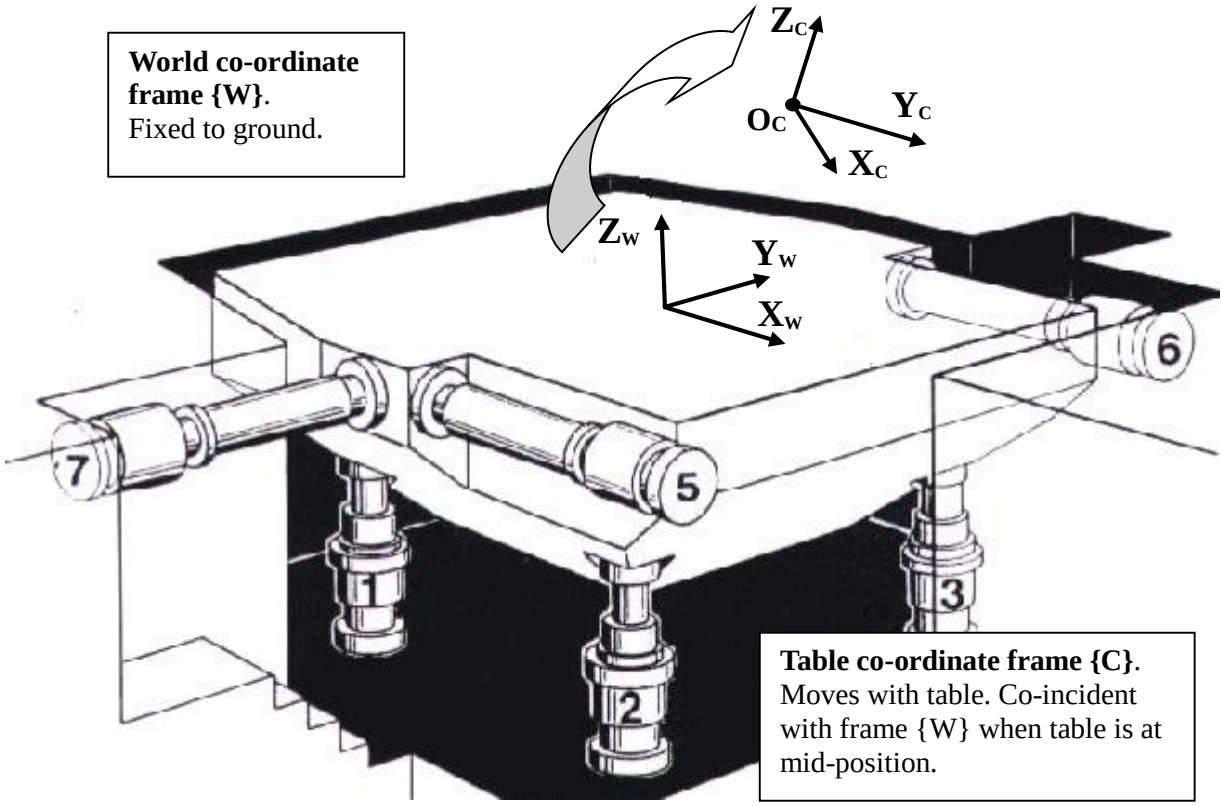

Fig. 12 Table co-ordinate frame definitions.

The 6 axes in this model will only be decoupled if $\mathbf{M^{-1}K}$ is diagonal, which in general is not the case. However transforming the displacements into some other co-ordinate system provides an opportunity to diagonalize $\mathbf{M^{-1}K}$. A linear transformation into 'modal displacements' $\mathbf{y_m}$ is given by

$$\mathbf{y_m} = \mathbf{P}^{-1}\mathbf{y_c} \qquad \mathbf{x_m} = \mathbf{P}^{-1}\mathbf{x_c}\,, \tag{24}$$

Thus giving

$$s^2\mathbf{y_m} + \mathbf{P}^{-1}\mathbf{M}^{-1}\mathbf{K}\mathbf{P}(\mathbf{y_m} - \mathbf{x_m}) = 0\,. \tag{25}$$

The 6x6 Matrix $\mathbf{P}$ should be chosen to diagonalize $\mathbf{P^{-1}M^{-1}KP}$. If $\mathbf{P}$ has as its columns the eigenvectors of $\mathbf{M^{-1}K}$, and the eigenvectors are linearly independent so that $\mathbf{P}$ is non-singular, then this diagonalization is achieved, and

$$\mathbf{P}^{-1}\mathbf{M}^{-1}\mathbf{K}\mathbf{P} = \mathbf{\Omega}\,, \tag{26}$$

where:

$$\mathbf{\Omega} = \begin{bmatrix} \omega_1{}^2 & & & 0 \\ & \omega_2{}^2 & & \\ & & \ddots & \\ 0 & & & \omega_N{}^2 \end{bmatrix}. \tag{27}$$

Each ω_i^2 term is the square of the natural frequency of one mode; these are the eigenvalues of $\mathbf{M^{-1}K}$. The modal decomposition described by equation (26) will always be possible, and efficient methods for calculating $\mathbf{P}$ exist; see [26] for details.

Define an Nx6 matrix $\mathbf{Q}$ which transforms the frame {C} table displacements into individual actuator displacements:

$$\mathbf{y} = \mathbf{Q}\mathbf{y_c}\,, \tag{28}$$

where $\mathbf{y}$ is the vector of N actuator displacements y_i. Thus referring to equation (24)

$$\mathbf{y} = \mathbf{R}\mathbf{y_m}\,, \tag{29}$$

where

$$\mathbf{R} = \mathbf{Q}\,\mathbf{P}. \tag{30}$$

Completing the system model, the valve dynamics and velocity gain (h) are assumed to be the same for each actuator. So

$$\mathbf{v} = V(s)\mathbf{u}\,, \tag{31}$$

where **u** is the vector of valve drive signals, **v** is the vector of spool positions, and *V(s)* is the scalar transfer function of equation (3) representing valve dynamics. Note that scaling factors and matching filters can be applied to the ultimate control signal to correct the velocity gain and valve dynamics for each actuator if they do differ. Combining equations (31) and (18) gives

$$\mathbf{x} = \frac{hV(s)}{s}\mathbf{u}, \tag{32}$$

and

$$\mathbf{x_m} = \frac{hV(s)}{s}\mathbf{u_m}, \tag{33}$$

where

$$\mathbf{u_m} = \mathbf{P}^{-1}\mathbf{u_c}. \tag{34}$$

From equations (25), (26) and (33), the complete model is

$$s^2\mathbf{y_m} + \mathbf{\Omega}(\mathbf{y_m} - \frac{hV(s)}{s}\mathbf{u_m}) = 0,$$

or

$$s(s^2\mathbf{I} + \mathbf{\Omega})\mathbf{y_m} = hV(s)\mathbf{\Omega u_m}. \tag{35}$$

This is diagonal, so each control loop can be designed independently based on scalar plant models of the form

$$y_{mi} = \frac{h\omega_i^{\,2}}{s(s^2 + b_i s + \omega_i^{\,2})}V(s)u_{mi}. \tag{36}$$

Note that a damping term b_i has been re-introduced: as damping is small it can be approximated by de-coupled terms. The complete multi-axis controller is shown in Fig. 13, in which $\mathbf{\hat{A}(s)}$ is an estimate of the multi-variable inverse actuator characteristic $\mathbf{A(s)}$ given by

$$\mathbf{A(s)} = \frac{1}{h}\mathbf{\Omega}^{-1}(s^2\mathbf{I} + s\mathbf{B} + \mathbf{\Omega}), \tag{37}$$

where **B** is the diagonal damping matrix containing elements b_i. With $N = 6$, **R** is a square matrix, and so its inverse can be used for the actuator to modal position conversion in the feedback path. The case for over-constrained systems ($N > 6$) is presented in Section 3.4.

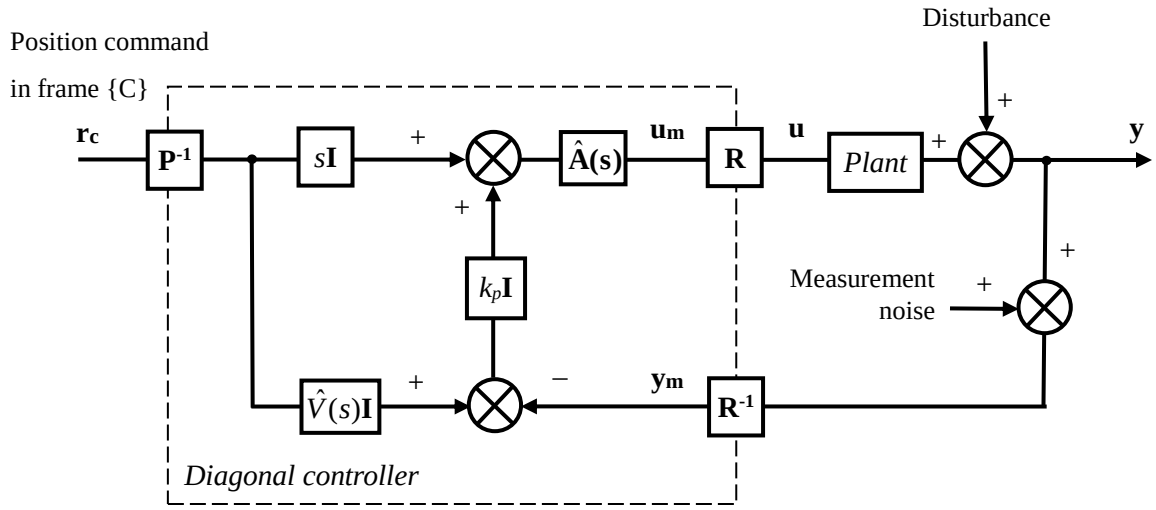

Fig. 13 The multi-axis decoupling controller (N = 6).

3.2 Mass and stiffness matrices

The linearised equation of motion for the combined table and payload is

$$ {}^{C}\boldsymbol{f}_t = \mathbf{M}\ {}^{C}\boldsymbol{a}_t , \tag{38}$$

where ${}^{C}\boldsymbol{f}_t$ is the vector of three orthogonal forces and three orthogonal moments acting on the table at frame {C}, ${}^{C}\boldsymbol{a}_t$ is the vector of three orthogonal linear accelerations and three orthogonal angular accelerations of frame {C}.

Define the mass matrix about the table/payload centre of gravity as

$$\mathbf{M}_{cg} = \begin{bmatrix} m_t\mathbf{I}_3 & 0 \\ 0 & \mathbf{I_t} \end{bmatrix}, \tag{39}$$

where m_t is the table plus payload mass, $\mathbf{I}_3$ is the 3x3 identity matrix, and $\mathbf{I_t}$ is the 3x3 matrix of moments and products of inertia. This needs to be transformed to frame {C}, and also the mass contributions from moving actuators and/or pushrods need to be added, giving

$$\mathbf{M} = \mathbf{M}_c + \sum_{i=1}^{N} \mathbf{J_i}^{-\mathbf{T}}\, \mathbf{M_{ai}}\, \mathbf{J_i}^{-\mathbf{1}} , \tag{40}$$

where $\mathbf{M_c}$ is the transformed table/payload mass matrix, the Jacobian matrices $\mathbf{J_i}$ relate actuator body velocities to table velocities, and $\mathbf{M_{ai}}$ are the actuator mass matrices. Derivation of mass matrices is discussed in [28].

The hydraulic stiffnesses referred to frame {C} are given by

$$\mathbf{K} = \mathbf{Q}^{\mathbf{T}} \begin{bmatrix} k_1 & & & 0 \\ & k_2 & & \\ & & \ddots & \\ 0 & & & k_N \end{bmatrix} \mathbf{Q}\,, \tag{41}$$

where k_i is the individual stiffness for each actuator.

3.3 Non-linear control

The controller compensates for some non-linear characteristics of the plant. In reality, the actuator stiffness varies with piston position according to equation (A28). Using this equation for each individual actuator stiffness, the stiffness matrix **K** is also time-varying. Thus the decoupling matrix **P** and the modal frequencies are recalculated at each controller time-step, giving time-varying inverse model, equation (37).

The variable gain in equation (16) can also be incorporated into the multi-variable controller. However the variable compensation is required on each individual valve control signal, u_i, rather than the modal control signals in vector $\mathbf{u}_m$. Thus the gain is constant in the inverse actuator model:

$$\hat{h} = \hat{H}_0\,, \tag{42}$$

but before each control signal is output u_i is scaled by

$$g_i(p_{acc}, \hat{f}_{hi}, u_i) = \frac{1}{\sqrt{\hat{r}_s\left(1 - \dfrac{\hat{f}_{hi}}{\hat{r}_s \hat{F}_{stall}}\operatorname{sgn}(u_i)\right)}}\,, \tag{43}$$

where each actuator hydraulic force $\hat{f}_{hi}$ is predicted from the product of the mass matrix and Cartesian command acceleration vector, subsequently transformed into actuator space. Individual valve control signals can also be scaled and filtered to correct for any differences in velocity gain and valve response.

The type of system under consideration has relatively small actuator strokes compared to the overall rig dimensions, and so the error in using a linear geometric transformation is small. However for maximum positional accuracy, precise non-linear inverse and forward kinematic calculations are used in the results which follow, rather than the linear transformation **Q** (which is a component of the transformation **R,** equation (30))

3.4 Force controlled axes

In the case where there are more actuators than degrees of freedom, i.e. $N > 6$, matrix **R** is non-square. Using the pseudo-inverse of **R** to calculate the modal displacements is a good choice as it gives the $\mathbf{y_m}$ which corresponds to an average of the measured actuator displacements (in a least squares sense):

$$\mathbf{y_m} = (\mathbf{R^T R})^{-1} \mathbf{R^T y} . \tag{44}$$

The system is now overconstrained, and a number of additional force control loops are required, equal to the number of additional actuators, to ensure that internal structural loads are small. As shown in Fig. 14, measured actuator forces **f** should be transformed by Nx(N-6) matrix **D** into N-6 'deformation forces'. The (N-6) x (N-6) matrix **C(s)** would typically be a diagonal proportional plus integral compensator. As discussed in detail in [28], the choice of matrix **D** is not unique, but it should be consistent with

$$\mathbf{Q^T D} = 0 . \tag{45}$$

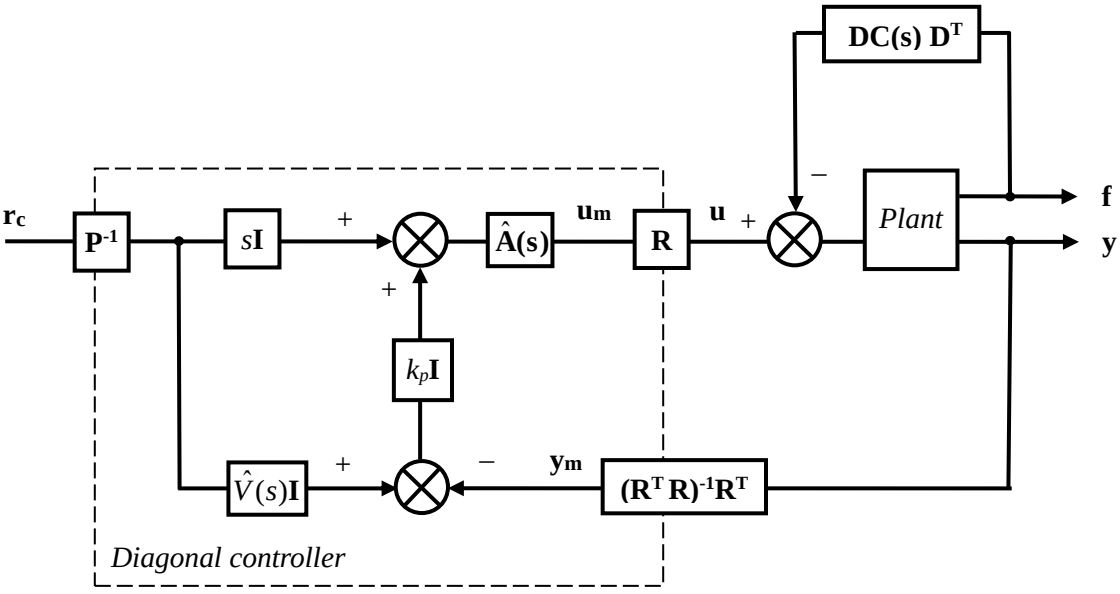

Fig. 14 The multi-axis decoupling controller for $N > 6$.

4. EXAMPLE

4.1 Example system

The shaking table of Fig.s 2 and 12 is used here as an example. It is a 6 DOF system driven by seven actuators. The table has a 5mx5m surface area and a payload capacity of 20 tonnes. The three horizontal actuators drive the table through pushrods; the cylinder bodies themselves are fixed. These actuators are equipped with 3-stage servovalves. The four vertical actuators are jointed at both ends, and are each equipped with four 2-stage servovalves. Ball joints are used throughout. The blind end of the double-ended vertical actuators are pressurised to support the dead weight of the table. Horizontal velocities of nearly 0.5 m/s can be achieved, and accelerations of over $10 m/s^2$. The intended test frequency range for this table extends up to 120Hz, functioning either in position or acceleration control. Key parameters for the hydraulic actuation system are given in Table 1. The hydraulic actuators, 3-stage servovalves, and mechanical hardware are design and manufactured by Instron Structural Testing (IST GmbH). The 2-stage servovalves are from Moog. The real-time controller platform is an Instron 8800 with Accelerator module for running auto-generated code from Mathworks' Simulink ®.

By choosing the frame {C} as shown in Fig 12, with its origin at the intersection of the lines of symmetry between the actuators in all three planes, then the matrix **Q** which relates table to actuator displacements (equation (28)) is given by

$$\mathbf{Q} = \begin{bmatrix} 0 & 0 & 1 & -L_v & L_v & 0 \\ 0 & 0 & 1 & -L_v & -L_v & 0 \\ 0 & 0 & 1 & L_v & -L_v & 0 \\ 0 & 0 & 1 & L_v & L_v & 0 \\ -1 & 0 & 0 & 0 & 0 & -L_h \\ -1 & 0 & 0 & 0 & 0 & L_h \\ 0 & 1 & 0 & 0 & 0 & 0 \end{bmatrix}. \tag{46}$$

The dimensions for this table, defined in Fig. 2(a), are L_v = 1.75m, L_h = 2.8m. From equation (45), a valid choice is

$$\mathbf{D} = \begin{bmatrix} 1 & -1 & 1 & -1 & 0 & 0 & 0 \end{bmatrix}^T, \tag{47}$$

which defines the deformation force axis. There is only one deformation axis as there is one degree of over-constraint. This force can be physically interpreted as twisting the table.

Table 1 Actuator parameters.

Parameter		**Value for actuators 1 to 7**		
		1-4	**5, 6**	**7**
Cylinder	Piston area (A), cm^2	74	127	220
	Stroke, mm	60	80	80
	Cylinder+manifold volume ($2V$), cm^3	630	1600	2670
	Internal leakage @ 70 bar, l/min	2.7	6	8
Valve	Rated flow @ 70 bar pressure drop, l/min	100	200	320
	Valve body flow @ 70 bar, l/min	560	600	1000
	Manifold flow @ 70 bar, l/min	300	400	1000
	Dead time (δ), ms	2	3.5	3.5
	Natural frequency (ω_{nv}), Hz	120	120	120
	Damping ratio (ζ)	0.7	0.7	0.7
	Slew rate limit, 100% per sec	200	200	200
	Overlap, %	0	0.7	1
Mechanical	Stiffness ($K_p^{-1} + K_m^{-1})^{-1}$, kN/mm	1030	426	664
General	Supply pressure (P_s), bar	275		
	Return pressure (P_r), bar	5		
	Estimated bulk modulus (B), GN/m^2	1.2		

The combined table and payload mass, m_t, is 43 000kg, and the moments of inertia are I_x = 134 000kgm^2, I_y = 114 000kgm^2 and I_z = 102 000kgm^2. With the payload in question, when the table is level the centre of gravity is vertically above the origin of frame {C}, at a height of h_c = 0.93m. The inertial contribution from the attached actuators/pushrods is small and will be neglected; the products of inertia are also small. This gives the mass matrix

$$\mathbf{M} = \begin{bmatrix} m_t & 0 & 0 & 0 & m_t h_c & 0 \\ 0 & m_t & 0 & -m_t h_c & 0 & 0 \\ 0 & 0 & m_t & 0 & 0 & 0 \\ 0 & -m_t h_c & 0 & I_x + m_t h_c^{\,2} & 0 & 0 \\ m_t h_c & 0 & 0 & 0 & I_y + m_t h_c^{\,2} & 0 \\ 0 & 0 & 0 & 0 & 0 & I_z \end{bmatrix}. \qquad (48)$$

The frame {C} origin is at the 'centre of stiffness' in this case, i.e. at a point where there is no cross-axis stiffness interaction. So the stiffness matrix **K** determined from equation (41) is diagonal. Elements vary with stroke, but at mid-stroke (when the table is at its nominal zero position), the stiffness matrix is

$$\mathbf{K} = \begin{bmatrix} 4.50x10^8 & 0 & 0 & 0 & 0 & 0 \\ 0 & 3.80x10^8 & 0 & 0 & 0 & 0 \\ 0 & 0 & 1.19x10^8 & 0 & 0 & 0 \\ 0 & 0 & 0 & 3.64x10^9 & 0 & 0 \\ 0 & 0 & 0 & 0 & 3.64x10^9 & 0 \\ 0 & 0 & 0 & 0 & 0 & 3.53x10^9 \end{bmatrix} \text{N/m.} \qquad (49)$$

From equation (10), this gives (at mid-position)

$$\mathbf{P} = \begin{bmatrix} 1 & 0 & 0 & 0 & -1.30 & 0 \\ 0 & 1 & 0 & 1.30 & 0 & 0 \\ 0 & 0 & 1 & 0 & 0 & 0 \\ 0 & -0.135 & 0 & 1 & 0 & 0 \\ 0.160 & 0 & 0 & 0 & 1 & 0 \\ 0 & 0 & 0 & 0 & 0 & 1 \end{bmatrix}. \qquad (50)$$

The decoupling matrix **R** can be derived as in equation (30), and the modal frequencies (at mid-position) are 15.2Hz, 14.1Hz, 8.4Hz, 27.8Hz, 30.5Hz and 29.6Hz respectively.

As proposed in section 3.4, matrix **C(s)** is a diagonal proportional plus integral controller, but in this case just has dimensions 1x1 as there is one degree of overconstraint. Both unity proportional and integral gains are used (where input and output signals have been non-dimensionalized by dividing by their maximum values), so

$$\mathbf{C(s)} = 1 + \frac{1}{s}. \qquad (51)$$

4.2 Simulation Results

Simulation results have been obtained using a detailed and well validated non-linear model of the system including valves, actuators and table [29]. Swept-sine horizontal acceleration responses have been acquired from which frequency responses are calculated. Note that acceleration commands are converted to position commands so that the position controller described in this paper can be used. Two aspects of the response are investigated:

1. the tracking response: *X*-direction command acceleration to achieved acceleration
2. the overturning sensitivity: *X*-direction command acceleration to pitch (θ) angular acceleration.

From Fig. 15 it can be seen that the bandwidth (-3dB point) is over 100Hz, and the worst case overturning sensitivity is -12dB (which is 0.25 rad/m). The gain used here is $k_p = 80$ (in fact the same gain is used for all modal motion control axes).

For comparison, the same plots are shown in Fig 16 for a proportional controller. Fig 17 shows the structure of this controller, for which the proportional loops are closed in frame {C} position co-ordinates, by using matrix **Q** (equation 46) to transform from actuator space. This approach is sometimes described as degree-of-freedom control, and is commonly used for this type of test rig [2]. As shown in the figure, a single deformation force loop is included, defined by **D** as given in equation (47), and with proportional force control **C(s)** reduces to a scalar constant, k_{pf}. The gains k_{p1} to k_{p6} and k_{pf} are tuned manually to give a fast response; $k_{pi} = 50$ for all i, and $k_{pf} = 1$. Now the bandwidth (Fig. 16) is around 15Hz and the response is highly oscillatory. The overturning sensitivity is about 1.0 rad/m. Fig. 18 compares the tracking response of the controllers in the time-domain, in response to a filtered step position command commencing at 0.005s; the step is filtered so that its first and second derivatives can be generated. The oscillation exhibited with proportional control would be reduced with a lower gain, but at the expense of even greater lag. The gains used are considered to be the maximum feasible gains which maintain adequate (though small) stability margins. The proportional gains used in the model-based controller are higher by a factor of 1.6 than the proportional controller gains but still with higher stability margins due to the modal actuator dynamic compensation, and the tracking response is further aided by feedforward rather than being solely reliant on the feedback path. Simply adding a feedforward path to the proportional controller is likely to improve the tracking response, particularly if the disturbance observer structure of Fig. 5 is used, but it would not reduce cross-coupling (e.g. overturning sensitivity), and would still exhibit an oscillatory response due to the uncompensated lightly damped resonant modes associated with the hydraulic actuator compliance.

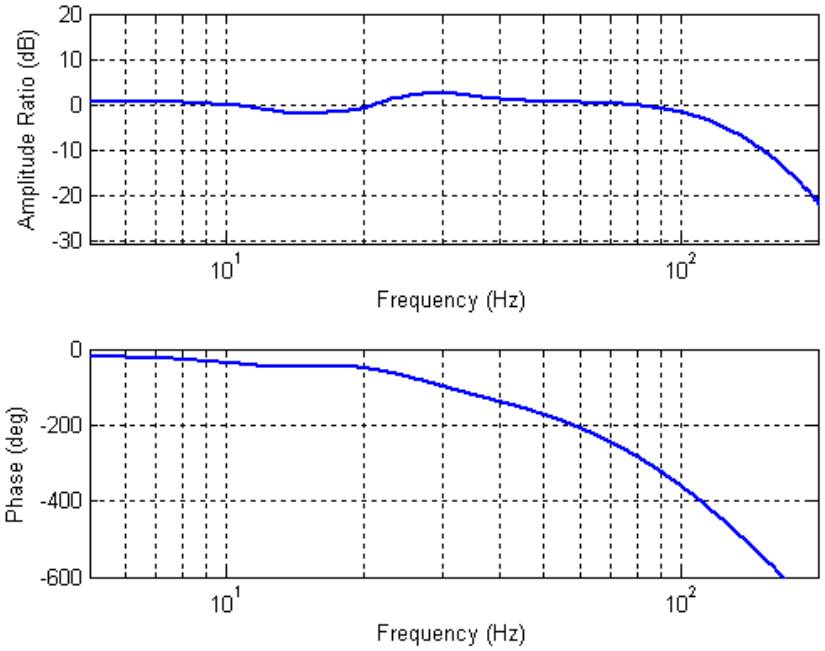

a) Tracking response (*X* direction acceleration).

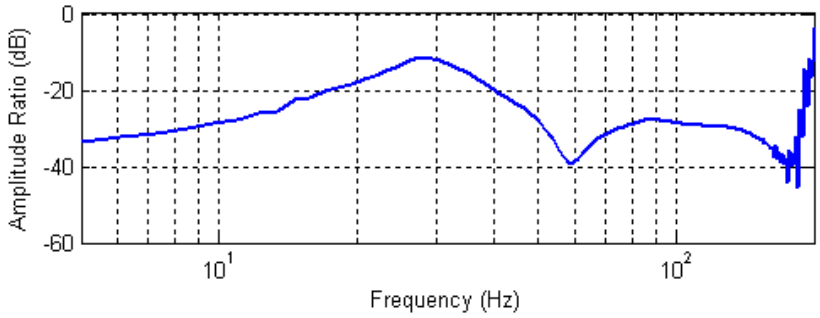

b) Overturning sensitivity (pitch over *X* acceleration command, rad/m).

Fig. 15 Simulation results for the model-based controller.

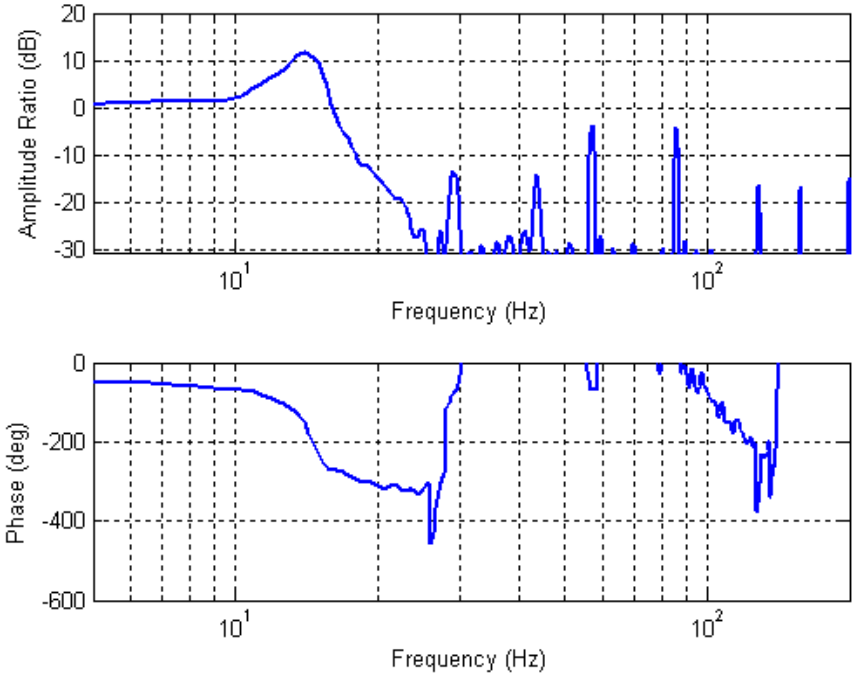

a) Tracking response (*X* direction acceleration).

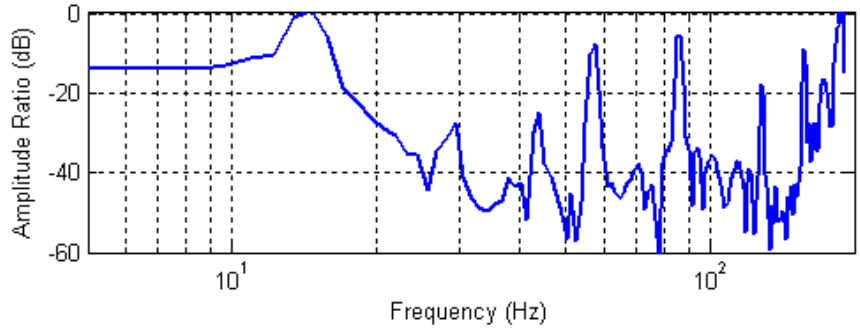

b) Overturning sensitivity (pitch over *X* acceleration command, rad/m).

Fig. 16 Simulation results for the proportional controller.

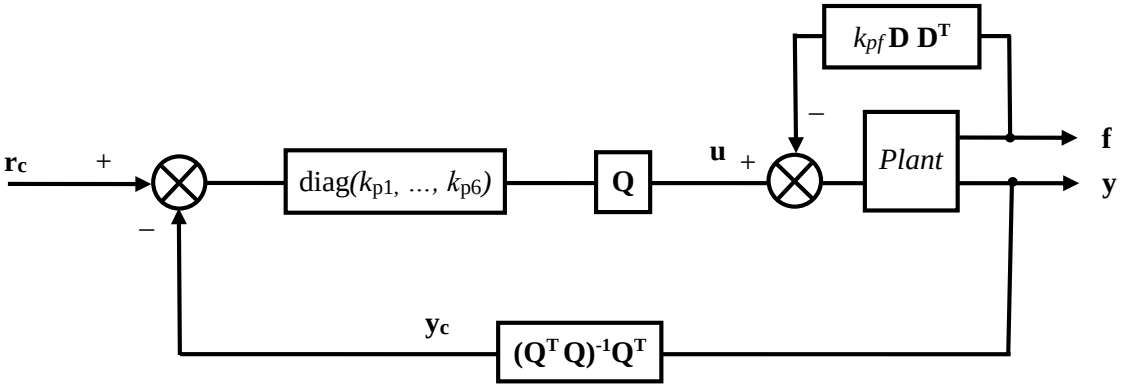

Fig. 17 The baseline multi-axis proportional controller.

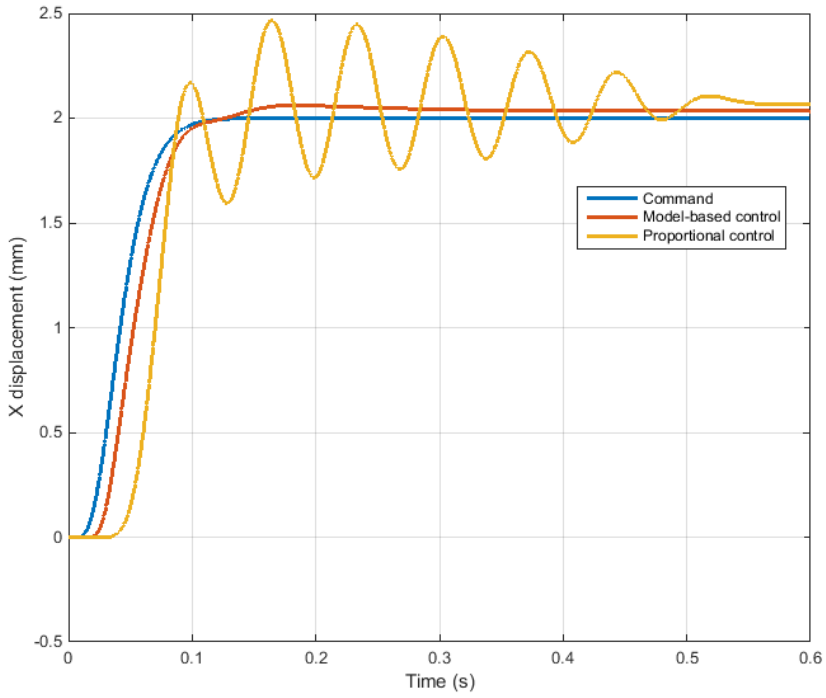

Fig. 18 A comparison of position responses to a filtered step command signal. (Command is a step filtered by a pair of second order lags, each with 100rad/s natural frequency and unity damping ratio)

Fig. 19 shows the model-based controller, but with the matrix **P** set to the identity matrix. Thus the modal decoupling is not achieved, and both the tracking response and overturning sensitivity are consequently inferior (particularly above 10Hz).

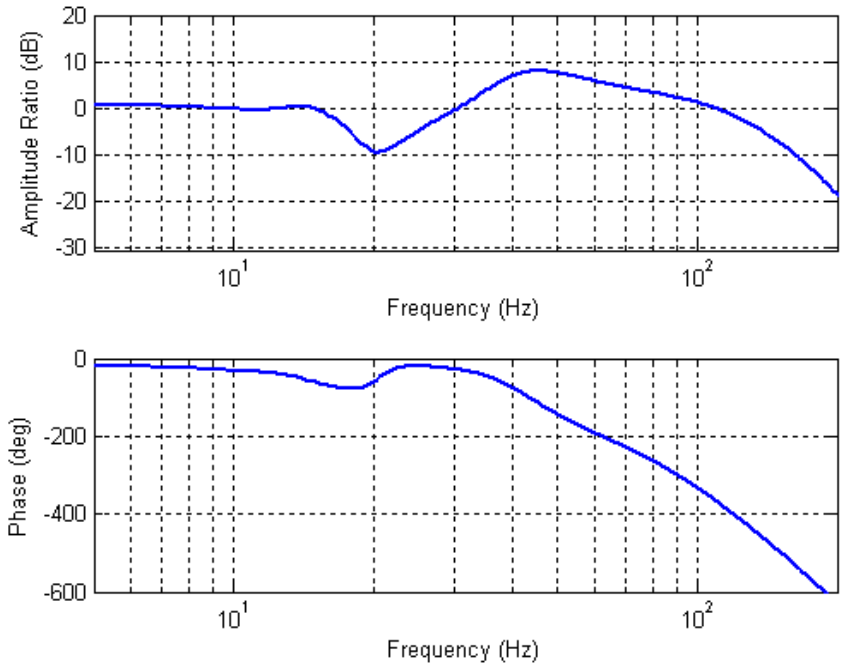

a) Tracking response (*X* direction acceleration).

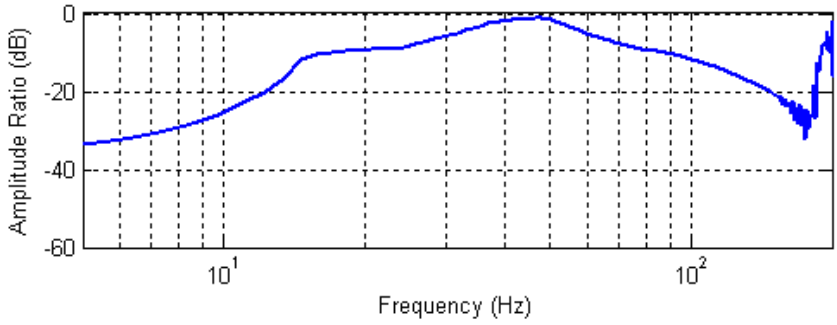

b) Overturning sensitivity (pitch over *X* acceleration command, rad/m).

Fig. 19 Simulation results for the model-based controller *without* decoupling.

4.3 Experimental results

Experimental results with the model-based controller have been obtained. As before, results are presented for the tracking response in the *X*-direction, and also the overturning (pitch) sensitivity to *X*-direction motion. Fig 20 shows the frequency response for the model-based controller compared to a proportional

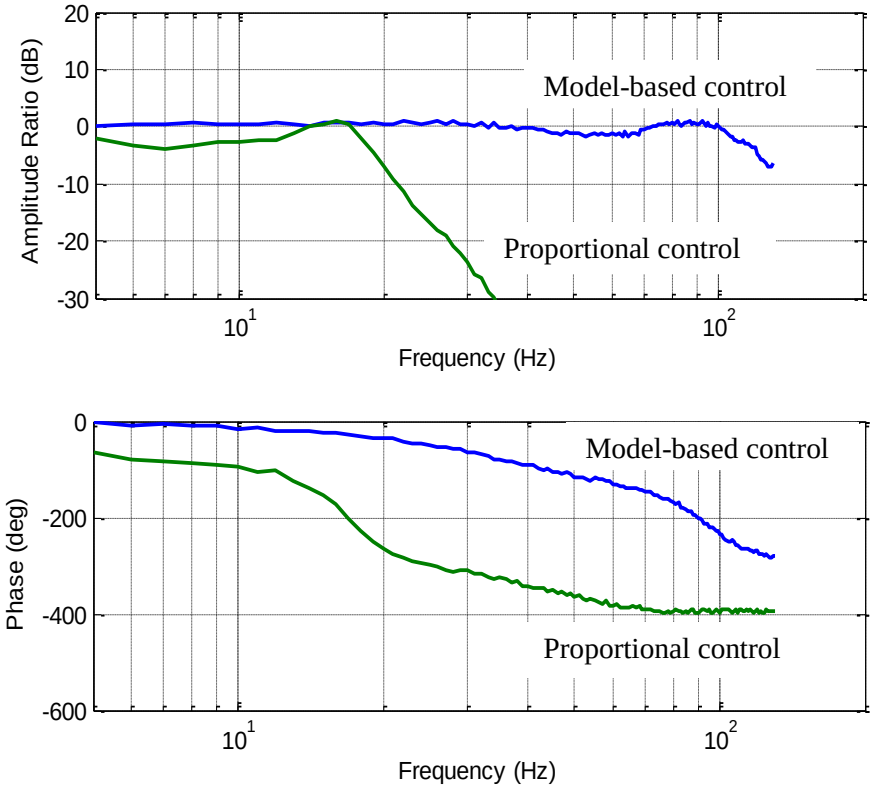

a) Tracking response (*X* direction acceleration).

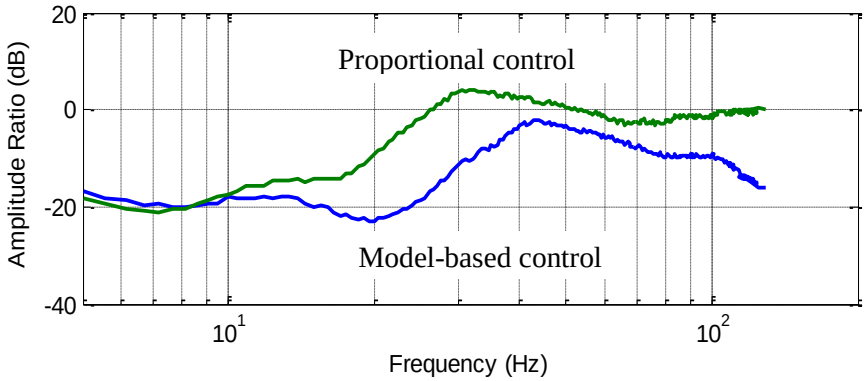

b) Overturning sensitivity (pitch over *X* acceleration command, rad/m).

Fig. 20 Experimental results for *X*-direction motion.

controller. The model-based controller has a bandwidth (-3dB point) well over 100Hz, and the worst case overturning sensitivity is -3dB. The proportional controller has a bandwidth of about 18Hz, and worst case overturning sensitivity of 4dB. The overturning sensitivity is very similar for the two controllers up to 10Hz, above which the model-based controller is better by between 5dB and 15dB (i.e. between a factor of 1.8 and 5.6). All six axes of control have been compared and similar improvements are found in every case. For example Fig. 21 compares the tracking response magnitude in the *Y* direction. As in simulation, all the proportional controller gains have been tuned manually to give a fast response, but the resulting gains are a little more cautious so the tracking resonant peak is lower.

Comparing figures 15 and 16 with 20, although there are differences between the simulation and experimental results (particularly in the case of the overturning sensitivity), the trends are similar, including the very significant improvement in the tracking response compared to proportional control. Note that in simulation, the proportional controller (Fig. 16) exhibits a tracking resonant peak and maximum overturning sensitivity at about 15Hz, which is the first modal frequency; from equation (50) it can be seen that this mode is dominated by X-direction motion. This resonant peak is eradicated by the model-based controller (Fig. 15), and the maximum overturning sensitivity is now at about 30Hz, which is the fifth modal frequency; this mode is dominated by pitch rotation. In the equivalent experimental results (Fig. 20), the proportional controller exhibits a resonant peak at a similar frequency (the first modal frequency) in the tracking response, but the peak overturning sensitivity is now at the fifth modal frequency. This difference results from errors in the modelling of coupling between the axes.

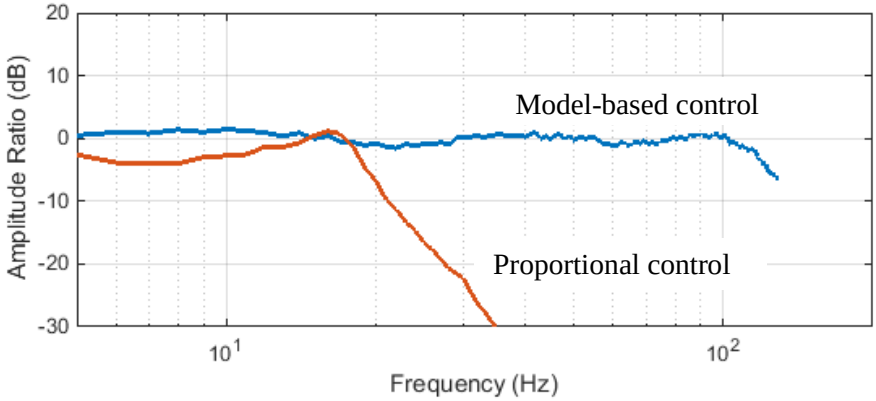

Fig. 21 Experimental results for *Y*-direction acceleration tracking response.

7. CONCLUSIONS AND DISCUSSION

A decoupling modal control approach has been described which could be applied to a range of multi-axis servohydraulic mechanisms with simple inertial loads. The model-based controller incorporates:

- command velocity feedforward, and proportional feedback of a disturbance estimate,
- an inverse actuator model to form an 'augmented plant' in which actuator dynamics are cancelled,
- non-linear compensation in the inverse actuator model in the form of a force dependent gain and variable actuator stiffness,
- decomposition of multi-axis dynamic behavior into separate modes in real-time, based on mass matrix (fixed) and stiffness matrix (variable with piston position),
- force control for redundant actuators to keep internal loads small,
- motion estimation based on an optimized combination of position and acceleration measurements.

Although the decoupling approach is (apart from variable stiffness), based on a linearised dynamic analysis, it is shown to work well for a large 6 DOF shaking table. In particular a favorable comparison is shown between the full controller with and without decoupling in simulation. Comparing the new controller with a proportional controller shows a very significant increase in performance; the bandwidth of the system is increased by a factor of 6. The proportional controller used has been tuned manually, and a high gain selected to maximize the performance, even though the response is a little under damped. Thus this 'base-line' controller has not been artificially de-tuned.

In practice, integral action may need to be added to the controller. Although this is not required when considering the table acceleration, for set-up and centering purposes accurate position control is still required. Due to steady effects such as valve null errors or inexact weight compensation, steady state position errors will inevitably result if integral action is not used, as evidenced by the final position error seen in Fig. 18.

Model-based controllers must be insensitive to modeling errors. Some preliminary robustness results are included in the paper, showing the effect of parametric errors in the augmented plant, and parametric errors in the inverse actuator model. The closed loop behavior is shown to be reasonably tolerant to parameter variation of ±20%. A more comprehensive robustness study is the subject of further work.

The complete controller is very complex compared to a proportional controller. Nevertheless, the controller is easily determined from plant model parameters. Many of these parameters can be found from known

physical data (e.g. piston areas, kinematics, some inertial data, hydraulic pressures etc.). Other parameters are best found empirically (e.g. valve transfer functions, mechanical stiffness). Detailed information about estimating model parameters can be found in [29]. A powerful real-time computer platform is required to implement the controller, but the cost of this is now very small compared to the complete system. A sample rate of 2.5kHz was used in this case.

The displacement range of this type of vibration or seismic testing table is often quite small, and so the geometric non-linearities would not normally be significant. For servohydraulic motion systems with a larger displacement range, such is flight simulator motion systems, the geometric linearization used here may not be applicable. However, the calculation speed of modern real-time computer systems is such that it would be feasible to calculate the decoupling matrix entirely on-line, and to use a linearized controller appropriate to the current local operating point. Since the current controller already re-calculates the decoupling matrix to account for varying stiffness, and uses accurate non-linear kinematic transformations to improve static accuracy, the additional computational overhead is not so great.

The objectives of achieving a high bandwidth and a high 'pitching stiffness' (insensitivity to inertial overturning moment) have been achieved, but only based on the assumption of the table and payload behave as a rigid body. In the case where the specimen has structural resonances within the test frequency range, the controller should still be applicable if the specimen mass is small compared to that of the table. However, for larger specimen masses, an alternative modal controller formulation would be required where the specimen flexibility is taken into account. Such a control strategy would be less convenient due to the detailed *a priori* specimen knowledge required.

ACKNOWLEDGEMENT

The author gratefully acknowledges ex-colleagues at Instron Ltd and IST GmbH for substantial assistance with this work.

REFERENCES

1. Ogawa, N., Ohtani, K, Katayama, T., Shibata, H. 2001 "Construction of a three-dimensional, large scale shaking table and development of core technology". Phil Trans R Soc Lond A, 359, pp. 1725-1751

2. Plummer, A.R.2007 "Control techniques for structural testing: a review" Proc. Instn. Mech. Engrs, Part I, Journal of Systems and Control Engineering, 221 (2), pp. 139-169.
3. Plummer, A. R., 2004 "Modal control for a class of multi-axis vibration table" Control 2004, Bath, UK, Sept 2004.
4. Plummer, A. R., 2007. "High bandwidth motion control for multi-axis servohydraulic mechanisms." In: ASME International Mechanical Engineering Congress and Exposition, Paper IMECE2007-412440, Seattle, USA, Nov 2007.
5. Kakegawa, T, Suzuki, T, Sato, E, Kajiwara, K, Tagawa, Y. 2003 "Linear model derivation and three-variable control (TVC) of the world's largest 3-D full-scale shaking table" Trans of the Japan Society of Mechanical Engineers, Part C, 69(2), 343-348 (in Japanese)
6. Kuehn, J., Epp, D., Patten, W.N. 1999 "High-fidelity control of a seismic shake table" Earthquake Engng. Struct. Dyn. 28, 1235-1254.
7. Yao, J, Dietz, M, Xiao, R, Yu, H, Wang, T, Yue, D. 2014 "An overview of control schemes for hydraulic shaking tables" Journal of Vibration and Control, pp1-17
8. Tagawa, Y., Kajiwara, K. 2007 "Controller Development for the E-defense shaking table." Proc. Instn. Mech. Engrs, Part I, Journal of Systems and Control Engineering, 221 (2), pp. 171-181.
9. Kajiwara, K., Sato, E., Mitsuta, T., Watanabe, S., Tagawa, Y. and Takai, S., 2003 "Design methodology of the three-variable control method for shaking-table control with acceleration feedback," Proc Fourth Symp. on Enhancement of Earthquake Performance of Infrastructures Based on Investigation into the Fracturing Process, Tokyo, pp.53-58, (in Japanese)
10. Xu, Y, Hua, H, Han, J. 2008 "Modeling and controller design of a shaking table in an active structural control system." Mechanical Systems and Signal Processing 22, 1917–1923
11. Philips, B.M., Wierschem, N.E., and Spencer, B.F. 2014 "Model-based multi-metric control of uniaxial shaking tables" Earthquake Engineering and Structural Dynamics 43(5), pp681-699.
12. Nakata N. 2010 "Acceleration trajectory tracking control for earthquake simulators" Engineering Structures 32(8), pp2229-2236.
13. Stoten, D. P. and Gomez, E., 2001 "Real-time adaptive control of shaking tables using the minimal control synthesis algorithm," Phil Trans R Soc Lond A, 359, pp1697-1723, 2001.
14. Shinohara, Y. and Shimizu, N. and Sato, E., 2004 "Experimental study on shaking-table control using adaptive control," Proc. American Soc. of Mech. Eng., Pressure Vessel and Piping Conference, Seismic Engineering, San Diego (CA), USA, pp.209-216,
15. Stoten D P, Shimizu, N 2007 "The feedforward minimal control synthesis algorithm and its application to the control of shaking-tables" Proc. Instn. Mech. Engrs, Part I, Journal of Systems and Control Engineering, 221 (3), pp. 423-444.

16. Shen, G, Zhu, Z.C., Zhang, L., Tang, Y., Yang, C.F., Zhao, J.S. *et al*.2013 "Adaptive feed-forward compensation for hybrid control with acceleration time waveform replication on electro-hydraulic shaking table" Control Engineering Practice 21(8), pp1128-1142.
17. Guan, G-F, Xiong, W, Wang, H-T. 2014 "Adaptive random control of a two-axis redundantly actuated electro-hydraulic shaking table" Journal of Vibration and Control.
18. Horiuchi, T, Dozono, Y, Konno, T 2001 "Improvement of accuracy of seismic acceleration waveforms of shaking tables by compensating for the reaction force in real time." Transactions, SmiRT16, Washington, August 2001.
19. Iwasaki, M, Ito, K, Kawafuku, M, Hirai, H, Dozono, Y, Kuosaki, K. 2005 "Disturbance observer based practical control of shaking tables with non-linear specimen." 16th IFAC World Congress, Prague, July 2005.
20. US Patent 4537077 "Load dynamics compensation circuit for servohydraulic control systems" MTS Systems Corporation, 1985.
21. Crewe, A.J., Severn, R.T., 2001 "The European collaborative programme on evaluating the performance of shaking tables." Phil Trans R Soc Lond A 359, 1671-1696.
22. Plummer, A R 2006 "A new acceleration feedback design method for electrohydraulic motion control systems". PTMC 2006, Bath, September 2006.
23. Edge, K.A., 2003, "On the control of electrohydraulic systems – some recent research contributions." The Eighth International Conference on Fluid Power, SICFP'03, Tampere, Finland, May 2003.
24. Skogestad, S, 2003 "Simple analytic rules for model reduction and PID controller tuning", Journal of Process Control, Volume 13, Issue 4, Pages 291-309
25. Plummer, A R. 2006 "Optimal complementary filters and their application in motion measurement" Proc. Instn. Mech. Engrs, Part I, Journal of Systems and Control Engineering, 220(6), 489-508, 2006.
26. Inman, D.J.1994 "Engineering Vibration" Prentice-Hall, New Jersey.
27. He, Jing-feng, Hong-zhou Jiang, and Zhi-zhong Tong, 2015, "Modal control of a hydraulically driven redundant actuated fully parallel mechanism", Journal of Vibration and Control doi:10.1177/1077546315596661.
28. Plummer,A. R., 2010, "A general co-ordinate transformation framework for multi-axis motion control with applications in the testing industry." Control EngineeringPractice, 18, 598–607.
29. Plummer, A. R., 2008. "A Detailed Dynamic Model of a Six-axis Shaking Table. Journal of Earthquake Engineering," 12 (4), pp. 631-662

APPENDIX – ACTUATOR MODEL

Flow – velocity relationship

An actuator is modelled driving a load of mass *m* as shown in Fig. 3. The figure also shows that the stiffness of cylinder mounting and load connection cannot be neglected [8]. The model includes fluid compressibility, leakage across the piston, and the valve orifice equations.

The cylinder flow equations are

$$q_1 = A\dot{z}_i + \frac{\dot{p}_1}{K_1} + (p_1 - p_2)C_l \tag{A1}$$

$$q_2 = A\dot{z}_i - \frac{\dot{p}_2}{K_2} + (p_1 - p_2)C_l \tag{A2}$$

and where the fluid stiffness on each side of the cylinder is $K_1 = \frac{B}{V_1}$, and $K_2 = \frac{B}{V_2}$, B being the bulk modulus; and C_l is the internal leakage coefficient.

Using the following approximation, which becomes exact at mid-stroke,

$$V_1 \approx V_2 \approx V \tag{A3}$$

$$K_1 \approx K_2 \approx K_{12} \tag{A4}$$

each side of the system is the same (symmetrical) and it can be shown that

$$q_1 = q_2 = q \tag{A5}$$

and

$$p_{acc} - p_1 = p_2 - P_r \tag{A6}$$

Thus summing (A1) and (A2) gives

$$q = A\dot{z}_i + \frac{\dot{p}_1 - \dot{p}_2}{2K_{12}} + (p_1 - p_2)C_l \tag{A7}$$

or

$$q = Asz_i + \left(\frac{1}{2K_{12}}s + C_l\right)\frac{f_h}{A} \tag{A8}$$

where *s* is the differential operator, and the hydraulic force is defined as

$$f_h = (p_1 - p_2)A \tag{A9}$$

Note that z_i is the relative displacement between piston and cylinder body, and from Fig. 3 it can be seen that this is related to the table displacement by

$$z_i = y_i + (\frac{1}{K_m} + \frac{1}{K_p}) f_h \tag{A10}$$

Substituting into equation (A8):

$$\frac{q}{A} = sy_i + \left(\frac{1}{k}s + \frac{C_l}{A^2}\right) f_h \tag{A11}$$

where combined mechanical and hydraulic compliance is

$$\frac{1}{k} = \frac{1}{2K_{12}A^2} + \frac{1}{K_m} + \frac{1}{K_p} \tag{A12}$$

Also, assuming that piston and cylinder body masses are negligible compared to the table mass, then

$$f_h = ms^2 y_i \tag{A13}$$

and so from equation (A11):

$$\frac{q}{A}k = s(ms^2 + cs + k)y_i \tag{A14}$$

where $c = \dfrac{mkC_l}{A^2}$.

Valve orifice equations

Given the function definition $\varphi(x) = \text{sgn}(x)\left|\sqrt{|x|}\right|$, the valve orifice equations are

$$q_1 = K_v v_i \varphi(p_{acc} - p_1) \qquad \text{for } v_i \geq 0 \tag{A15}$$

$$q_1 = K_v v_i \varphi(p_1 - P_r) \qquad \text{for } v_i < 0 \tag{A16}$$

$$q_2 = K_v v_i \varphi(p_2 - P_r) \qquad \text{for } v_i \geq 0 \tag{A17}$$

$$q_2 = K_v v_i \varphi(p_{acc} - p_2) \qquad \text{for } v_i < 0 \tag{A18}$$

where v_i is the valve spool displacement. Assuming that $(p_1 - p_2) \leq (p_{acc} - P_r)$, using the symmetry argument gives

$$q = K_v v_i \sqrt{\left(1 - \frac{p_1 - p_2}{p_{acc} - p_r}\text{sgn}(v_i)\right)\frac{(p_{acc} - P_r)}{2}} \tag{A19}$$

or

$$q = K_v v_i \sqrt{\left(1 - \frac{f_h}{r_s F_{stall}}\text{sgn}(v_i)\right)\frac{r_s(P_s - P_r)}{2}} \tag{A20}$$

where

$$F_{stall} = (P_s - P_r)A \tag{A21}$$

and

$$r_s = \frac{p_{acc} - P_r}{P_s - P_r} \tag{A22}$$

Gathering together the constant terms in (A20):

$$\frac{q}{A} = hv_i \tag{A23}$$

where

$$h = H_0\sqrt{r_s\left(1-\frac{f_h}{r_s F_{stall}}\operatorname{sgn}(v_i)\right)} \tag{A24}$$

and H_0 is a constant:

$$H_0 = \frac{K_v}{A}\sqrt{\frac{P_s - P_r}{2}} \tag{A25}$$

If the hydraulic force is small compared to the actuator stall force, and the accumulator is near full charge (i.e. $p_{acc} \approx P_s$, so that $r_s \approx 1$) then $h \approx H_0$.

Complete single actuator model

Combining equations (A14) and A(23), the relationship between valve spool displacement and table displacement can be expressed as

$$s(ms^2 + cs + k)y_i = hkv_i \tag{A26}$$

This is linear if $h = H_0$ is used, or non-linear if h is given by equation (A24). Another non-linearity which can be important is the variation in stiffness with piston position. This has been neglected by assuming a constant, equal volume either side of the piston, as in equations (A3) and (A4). In reality, the stiffness varies with piston position according to:

$$K_1 = \frac{B}{V + Az_i}, \text{ and } K_2 = \frac{B}{V - Az_i} \tag{A27}$$

and so equation (A12) can be rewritten as

$$\frac{1}{k} = \frac{1}{K_1A^2 + K_2A^2} + \frac{1}{K_m} + \frac{1}{K_p} \tag{A28}$$

Here V is the volume trapped between one side of the piston and the valve at mid-stroke.